Determination of Total Organic Carbon content using Passey's ΔLogR method in coals of the Central Kalahari Karoo Basin, Botswana.

Mamphedi Sylvia Mabitje

A Minithesis submitted in partial fulfilment of the requirements for the degree of Master of Science in the Faculty of Science, Department of Earth Science, University of the Western Cape.

Supervisor: Dr Mimonitu Opuwari

October 2015

ABSTRACT

The Kalahari Karoo Basin is one of several basins in southern Africa filled with Late Carboniferous to Jurassic sediments that are primary targets for Permian aged coal. In order to determine the Coalbed Methane (CBM) potential of the Central Kalahari Karoo Basin, 9 exploration boreholes were drilled. Vitrinite reflectance (%Ro) and proximate analysis were conducted on cored coal intervals. Passey's ΔLogR method used in this thesis employs the use of resistivity and porosity logs to identify and quantify total organic carbon (%TOC) in potential source rocks.

Compared with lab measured %Fixed Carbon, the results showed that Passey's ΔLogR method effectively identifies coal intervals as organic enriched. In terms of %TOC calculations, the method works poorly in coal metamorphosed by dolerite intrusions. These heat affected coal samples display %Ro from 0.77% to 5.53% and were increased in rank from primarily sub-bituminous to higher ranking volatile bituminous and finally to anthracitic coal. Their higher level of organic metamorphism (LOM), accompanying compositional changes and increased density associated with accelerated coal rank seem to have hindered the method in its estimations or lack thereof. Compositional changes in the coal were controlled by proximity to sill intrusion, with a decrease in fixed carbon and volatile matter, and increases in ash and moisture in the contact metamorphism zone (2-12m from sill).

In heat unaltered coal that has undergone normal burial maturation characterized by %Ro of 0.44% to 0.65%, the method works very well even attaining accuracy in some samples. In unintruded boreholes CH1 and CH6, correlations between fixed carbon and generated %TOC curves indicate strong relationships with R^2 from 0.70 to 0.83. Therefore, it was found that Passey's ΔLogR method can be applied effectively on coal that has undergone normal burial maturation only.

DECLARATION

I declare that *Determination of Total Organic Carbon content using Passey's ΔLogR method in coals of the Central Kalahari Karoo Basin, Botswana* is my own work, that it has not been submitted before for any degree or examination in any other university, and that all the sources I have used or quoted have been indicated and acknowledged as complete references.

Mamphedi Sylvia Mabitje October 2015

Signed: _____

ACKNOWLEDGEMENTS

I would like to sincerely thank my supervior, Dr Mimonitu Opuwari for his guidance and support. I would like to extend my sincere gratitude to Christopher McLean for his guidance and dedication. I would like to thank Sasol Exploration and Production International (SEPI) for providing me this opportunity to study further. I would like to thank Hanno van Staden and Ben Egbe for their support. I am grateful to my advisor at SEPI, Junior Potgieter for his encouragement and data provisions needed to complete this study.

I would also like to thank my family for their love, encouragement and unceasing support. Without you all, this project wouldn't be anywhere.

Table of Contents

1. Introduction

Coal is increasingly becoming an exploration target in many basins across the world, since it has recently been accepted as a potentially significant hydrocarbon generating source (Ogala, 2011). Kubu Energy acquired coal prospecting licences for three blocks (Figure 1) within the Central Kalahari Karoo Basin, Botswana. Exploration in the basin revealed that methane concentrations in the coal seams of the Morupule and Serowe formations are under-saturated. Desorbed gas contents range between <1 and ≈2 m3/t, with a few higher readings associated with dolerite intrusions (Faiz et al., 2013).

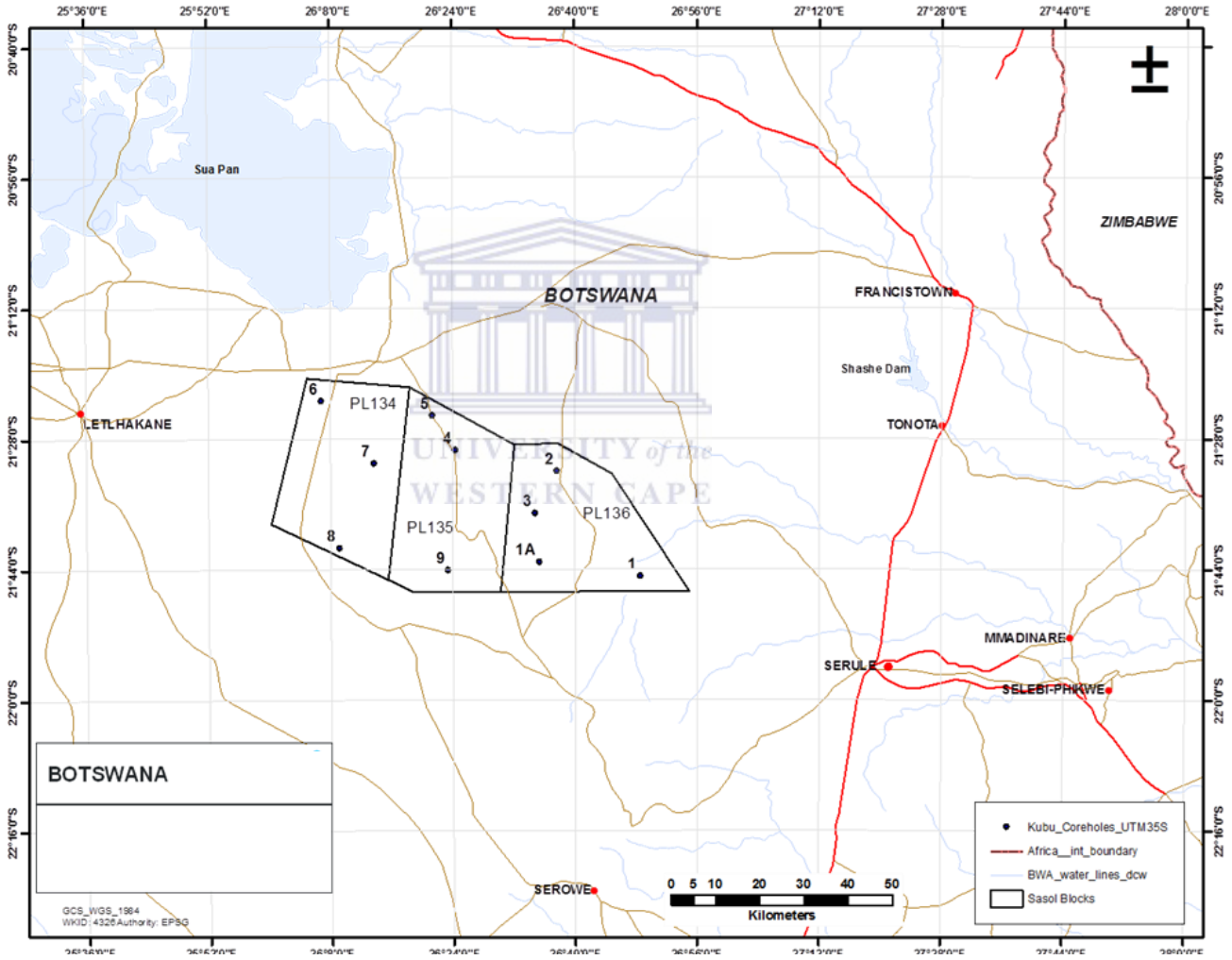

Figure 1: Location of the 9 exploration boreholes in central Botswana within acquired coal prospecting licenses (PL) (134/2010, 135/2010 and 136/2010) in an area extending over approximately 3,000 km^2.

Wireline logs are used as an inexpensive and available method to extract information relating to the subsurface conditions and rock properties. It is common practice to use amongst other methods, Passey's ΔLogR technique, to evaluate total organic carbon (%TOC) using resistivity and porosity logs (Passey et al., 1990; Shiri et al., 2013). In industry, application of Passey's ΔLogR technique has proven to be an effective approach for estimating %TOC content in source rocks (Passey et al., 1990).

This study will attempt to determine if Passey's method is able to identify coal bed methane (CBM) bearing rocks of the Central Kalahari Karoo Basin, as organic carbon rich zones. This method will also be used to attempt to quantify the %TOC in the coal bearing formations. Passey's calculated %TOC will be compared to the fixed carbon measurements from the proximate analysis, to test the validity of this technique.

Data available for this study included wireline logs, geological logs, proximate analysis results and vitrinite reflectance measurements for exploration boreholes CH1 to CH9. However, vitrinite reflectance measurements were not conducted on all cored intervals; only 4 to 5 samples were selected per borehole. Since Rock-Eval pyrolysis was not conducted on the coal samples, vitrinite reflectance will be used to determine their thermal maturity as this is an important parameter in the %TOC calculations.

2. Regional Geology

The Kalahari Karoo Basin is one of several southern African Karoo Basins filled with Late Carboniferous to Jurassic sediments that are primary targets for Permian age coal. The basin covers approximately 70% of Botswana (Figure 2), trending Northeast-Southwest. It is divided into five sub-basins based on geological setting and facies changes (Smith, 1984). The Central Kalahari Karoo Basin is further sub-divided into Southern, Northern, Western and South East Central Kalahari Belts for descriptive purposes (Smith, 1984). The area of focus for this study is within the Northern and South East Central Kalahari Belts indicated in Figure 2.

Deposition of the Karoo Supergroup in the basin occurred in relatively shallow depressions formed as a consequence of the pre-existing relief of the rigid cratonic basement and suggested syn-Karoo faulting. As a result, variable thickness and a generally south–southwest thickening succession (from approximately 1000 m in the north to approximately 1500 m in the south-west) of strata has been inferred (Segwabe, 2008). Sediments of the Cenozoic Kalahari Group filled the basin, except for a few poor exposures on the eastern and north eastern basin fringes (Smith, 1984; Bordy et al., 2010).

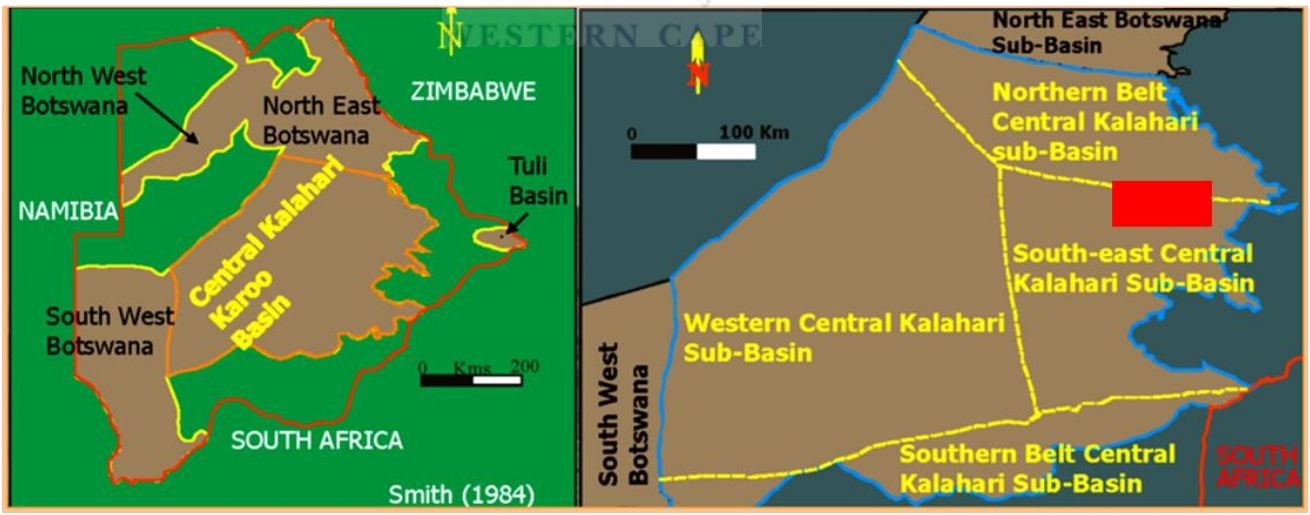

Figure 2: (Left) Location of the central Kalahari Karoo Sub-basin. (Right) Subdivisions of the central Kalahari Karoo Sub-basin (Adapted from Segwabe, 2008). Red block indicates total acreage of licenced blocks where borehole studies were conducted.

2.1 Tectonic Evolution

The Kalahari Karoo Basin and its subsidiary basins remain little understood in terms of their exact geodynamic setting. Some studies, namely Visser (1997), Haddon (2005) and Catuneanu et al. (2005) have attributed the origin of these sub-basins to collision induced extensional tectonics, related to the Late Palaeozoic to Early Mesozoic Gondwanide-Cape orogeny that resulted from the subduction of a palaeo-Pacific plate under southern Gondwana. This led to the development of the Karoo Basin in the south as a retro-arc foreland basin to the Cape Fold Belt (Figure 3). During this period the Kalahari Karoo Basin, and other subsidiary basins, developed in the north as intracratonic sag or rift basins (Catuneanu et al., 2005; Modie, 2008). The tectonic evolution of the Karoo Basin can be divided into various stages: (1) Pre-Dwyka shortening and regional uplift as evidenced by the regional stratigraphic hiatus, succeeded by (2) Dwyka to Ecca intracratonic platform sag (Visser, 1997).

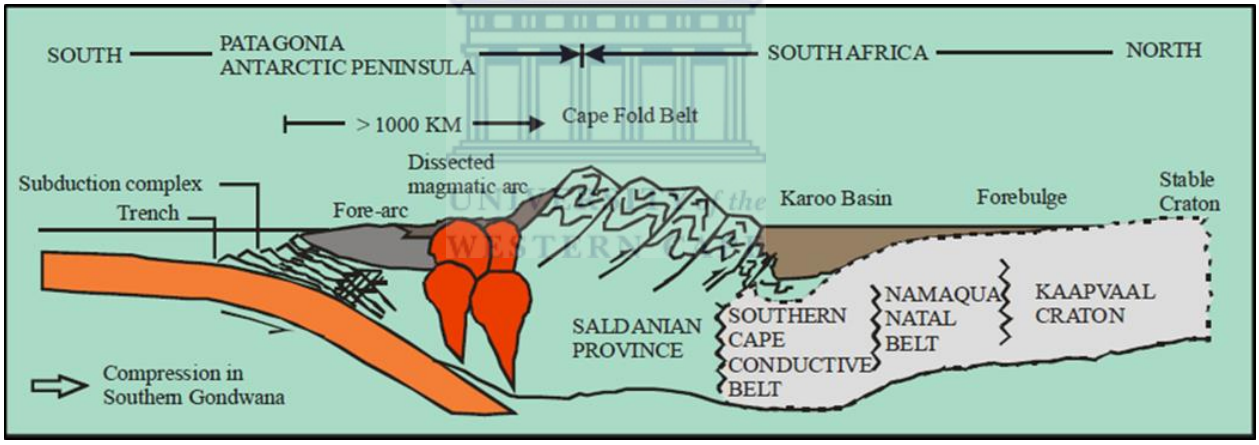

Figure 3: Geodynamic setting of the Main Karoo Basin as a foreland basin to the Cape Fold-belt orogeny (Modie, 2008; Segwabe, 2008).

2.2 Structural Development

The sub-surface structural framework of the Kalahari Karoo Basin is little understood due to the extensive nature of the Kalahari Desert sediments, which are generally 60-100m thick generally and can reach 400m thickness in the central Kalahari (Rainbow Gas & Coal, 2012). Fault-bounded graben structures have been identified along the eastern margin of the basin, where it is exposed on the surface. The use aeromagnetic and seismic data to define main structural elements such as lineaments and faults, has confirmed a rift basin setting for covered interior parts of the Kalahari Karoo Basin (Modie, 2008). Pre-Karoo (Archaean, Proterozoic aged) structural elements seem to have had an influence on the structural

evolution of the Kalahari Karoo Basin as evidenced by the close relationship between basin disposition and major interpreted geophysical lineaments (Figure 4). These lineaments include the Makgadikgadi Line, Kalahari Line, Zoetfontein Fault and fault lines associated with the Pan African Ghanzi-Chobe Belt which are generally parallel to major boundaries that define segments of the Kalahari Karoo Basin (Modie, 2008).

2.3 Dolerite Intrusion

The dyke swarm in central Botswana represents one of the major fissure intrusive complexes in the world (Le Gall et al., 2002). This complex forms a 1500 km long and 100 km wide tectono-magmatic structure extending from western Zimbabwe through Botswana and into northern Namibia. The strike of dyke complex trends at 110° east. The individual dyke intrusions dip between 60 and 90 degrees to the north-east. Studies show that the dykes intruded between 179.6 and 181 Ma, these dyke intrusions cut through Archaean basement terranes and Permo- Jurassic sedimentary sequences (Le Gall et al., 2002).

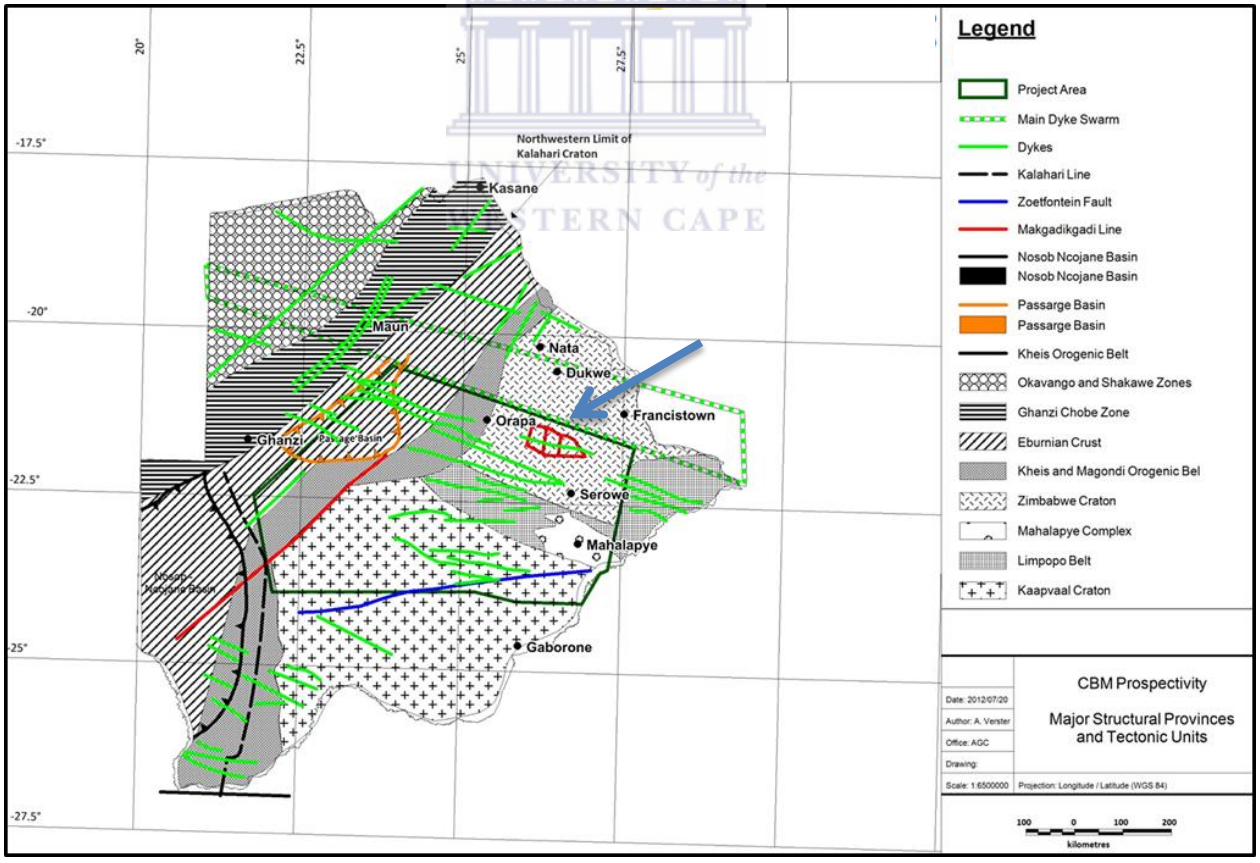

Figure 4: Major structural elements and tectonics units of Botswana (Andersen and Potgieter, 2012). The three prospective blocks in the study area are indicated as a red outline.

2.4 Stratigraphy

The stratigraphy (Figure 5) of the Kalahari Karoo Basin records a transition from a glacial period through to fluvio-deltaic and swampy periods and ultimately turning arid before the extrusion of continental flood basalts (Smith, 1984; Visser, 1997). Stratigraphic nomenclature of the Kalahari Karoo Basin is largely adopted from the South African Karoo stratigraphy, owing to correlation with the better-exposed and studied main Karoo Basin (Smith, 1984; Catuneanu et al., 2005; Bordy et al., 2010).

- Dukwi Formation

The glacially influenced Dukwi Formation, which is the equivalent of the Dwyka Group, unconformably overlies pre-Karoo basement and was deposited approximately 300 Ma (Catuneanu *et al.,* 2005). Deposition generally begins with a basal tillite, followed by pale sandstone that fines up into banded siltstones and is overlain by a varved siltstone or mudstone sequence with dropstones (Smith, 1984).

- Ecca Group

Deposited approximately 288 ± 3 Ma, the Ecca Group lies unconformably on underlying Dukwi sediments and comprises of fluvial deltaic and coal swamp facies (Catuneanu et al., 2005). The lower Ecca group (≈107 m thick) consists of a sequence of medium to fine grained sandstones and siltstones. The middle Ecca Group (≈165 m thick) is characterized by white and yellow, meduim-grained feldspathic sandstones with a frequent occurrence of coal seams towards the eastern part of the country. These coal seams diminish westwards leading to dominance of the sandstones. The upper Ecca is characterized by a sequence of alternating carbonaceous clays with coals and sandstones (Smith, 1984; Bennett, 1989).

The middle and upper Ecca Group host the important coal bearing formations, namely the Serowe and Morupule Formations with maximum thicknesses of 50 m and 70 m, respectively (Bennett, 1989; Smith, 1984). Deposition of the Morupule formation is suggested to have occurred in a quiet environment with accumulation of organic and argillaceous material in a swamp or floodplain. Whereas peat accumulation in a low-relief environment with very stable shallow water conditions is suggested for the Serowe formation (Smith, 1984; Bordy et al., 2010).

- Tlhabala Formation

The Tlhabala formation is equivalent to the Beaufort Group of the main Karoo Basin. It overlies the Ecca Group and was deposited during the Late Permian- Early Triassic (Haddon, 2005). It is bound above and below by unconformities which according to Haddon (2005), were due to erosion that was a consequence of syn-depositional regional uplift. It consists of pale grey mudstones, sandstones, siltstones and thin limestone beds (Smith, 1984). Sediment deposition occurred in a lacustrine/ flood-plain type setting controlled by down-warping and faulting (Haddon, 2005).

- Lebung Group

The Late Triassic-Early Jurassic Lebung Group equates to the Molteno, Eliott and Clarens Formations of the main Karoo Basin. This group includes clastic red bed formations deposited unconformably on the Tlhabala or earlier formations (Haddon, 2005). This group is divided into the lower Mosolotsane and upper Ntane formations. Mosolotsane Formation consists of a fining up sandy facies, red siltstones and mudstones. The depositional environment for this formation is proposed to be one in which fluviatile terrestrial conditions prevailed, with red colouration developed through diagenesis indicative of long periods in semi-arid conditions. The Ntane formation comprises mainly of massive fine grained sandstone thought to have been deposited desert environment, dominated by clastic aeolian sedimentation (Smith, 1984).

- Stormberg Lava Group

The Stormberg Lava Group serves as the youngest group in the Karoo Supergroup, and its K-Ar age determination yields ages between 179.6 and 181 Ma (Le Gall et al., 2002). Extrusion of continental flood basalt occurred as a result of the breakup of Gondwana (Catuneanu et al., 2005). It is the stratigraphic equivalent of the Drakensberg Group of South Africa. Throughout the Basin, the Stormberg Lava Group is unconformably overlain by the Kalahari Group which comprises Late Cretaceous to recent sediments in age (Smith, 1984).

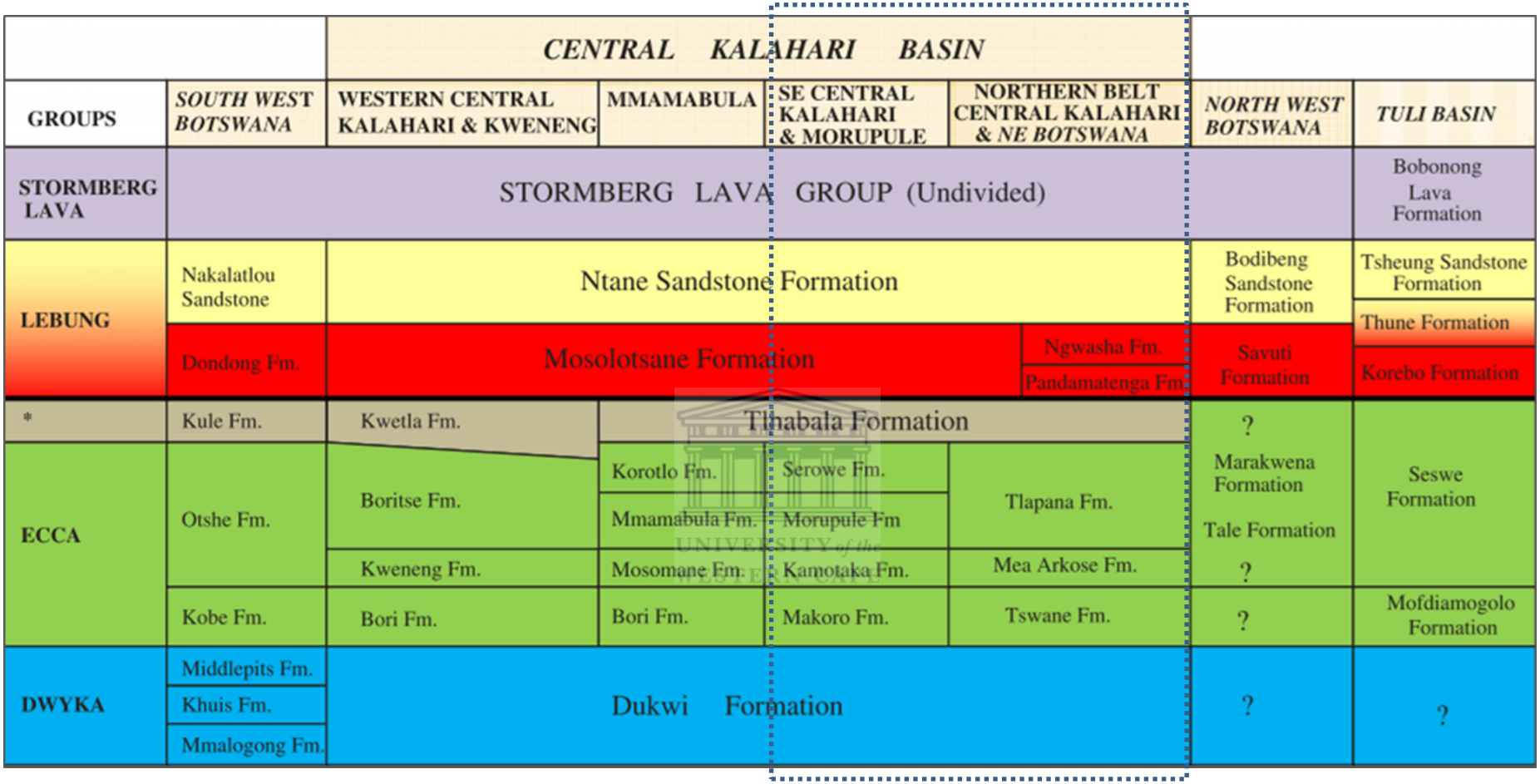

Figure 5: Central Kalahari Basin Lithostratigraphy. The asterisk denotes a non-carbonaceous sequence lacking assertive palaeontogical and lithological evidence hence its correlation with the Beaufort Group of the main Karoo Basin is uncertain. Thick black line shows the regional unconformity at the base of the Lebung Group separating the Karoo Supergroup into the informal lower and upper sequences. Blue box highlights the study area (Bordy et al., 2010).

2.4.1 Detailed Description of Target Formations

The logging results by Smith (1984) of boreholes drilled by Shell Coal in central and south Botswana are presented. Borehole C165 (Figure 6) provides a comprehensive generalized lithostratigraphy of the Morupule and Serowe formations described below.

Morupule Formation

Being the main target formation of this study, the Morupule Formation hosts thick dull Permian coal seams, which includes the Morupule Main seam mined at the Morupule colliery. In the south eastern Central Kalahari sub-Basin this formation is widespread throughout, however it is more developed in the Morupule coalfield area that it was named after. It overlies carbonaceous mudstones of the Kamotaka Formation. The Morupule Formation has been divided into three members (and their corresponding sub members) based on the level of development of the coal seams in the Morupule coalfield.

- *Member F1*

Member F1 lies between 304.7 m -285.1 meters from the surface. It consists of a thick coal zone which in the Morupule coalfield is divided into two sequences by a middle carbonaceous mudstone sub-member known as F1b. F1a is the lower coal sequence that is thought to be one seam; the Morupule main seam of dull coal that grades into a heavy dull coal consisting of silty mudstone partings of a few centimetres thickness. The seam is rich in intertite with scattered pyrite nodules. Minor carbonate coatings occur on cleats in the brighter vitrainous bands formed within a metre of the top and bottom of the seam. The seam is encountered from 304.7m to 298.3 m and has within it an irregular limestone band approximately 13 cm thick. Within cleats of brighter bands are carbonate coatings.

Overlying the F1a sub-member is F1b from a depth of 298.3 m to 293.3 m. This member is mainly a black carbonaceous mudstone with incorporated thin dull coals and lenses of brighter coal. Succeeding this sub-member is a sequence that makes up F1c and F1d comprising dull and heavy dull coals with thin coaly mudstone bands. This sequence continues until the top of F1 at 285.1 m. The seams in F1c and F1d are not borehole developed as F1a and their limited thickness requires petrophysical logs to differentiate sub-members.

- *Member F2*

Member F2 lies between 285.1 m and 254.6 m, the entire sequence comprises black carbonaceous mudstones and thin heavy dull coals with bright coal discontinuous veins. Between 263.2 m and 263.3 m, a 10 cm greyish brown shaly limestone band occurs. The coal beds are mainly in the form of lenses with gradational boundaries implying that part of F2 seems to have been eroded along the axis of the Makoro Trough; and replaced by channel sandstones. These sandstone wedges in the Morupule coalfield thin towards and are confined to the upper F2.

- *Member F3*

This member is essentially top of the Morupule Formation lies between 254.6 m and 239.9 m accumulating a thickness of 14.62 m. Sub-member F3a also named the Mosolotsane Seam comprises 2.65 m thick of generally bright coal (254.6 m- 251.9 m). Outside the Morupule coalfield vicinity F3a varies in thickness and quality consisting of thin coal seams interbedded with carbonaceous mudstone. These F3 coals show a tendency to decrease in quality and thickness upwards. Between 251.9 m and 239.9 m there is approximately 12 m of thin intercalated bright coal or siltstone stringers within the dominant carbonaceous mudstone.

Deposition of the Morupule Formation is suggested to have occurred in a quiet environment where accumulation of organic and argillaceous material in a swamp or floodplain. There seems to have been a depositional break after the Kamotaka sandstone that was most likely due to sands building out laterally whilst subsidence was relatively slow. This created favourable conditions for a thick layer of peat to accumulate to collect in swampy plains. An increase in subsidence rates and terrigenenous sediment inflow was responsible for the channel sandstone and muddy overbank during F2 deposition while during F1, little clastic material was introduced onto the swamp plains and limestones were deposited in a few small channels.

Serowe Formation

In the south-eastern part of the central Kalahari Sub-basin, The Serowe Formation can be seen where its base is the bottom of the pale grey siltstone and fine grained sandstone

marker beds and its top is the junction of the youngest coal or coaly shale with overlying generally non-carbonaceous mudstone and marls. This formation comprises three members. They can be defined between 239.9 m and 199.3 m acquiring a total thickness of 40.7 m.

- *Member G1 (239.9 m- 231.2 m)*

The base of a light grey siltstone overlies mainly carbonaceous mudstone and the top of the siltstone sequence is considered to be from where black carbonaceous mudstones and coals predominate. At 239.9 m and 231.2 m it consists of pale grey siltstones, these pale grey siltstones include a 1.65 m central band of sandy siltstones with lenses of a calcareous nature. The top of the member comprises greyish brown siderite pellets with siltstone lenses. These siltstones are generally finely laminated, micaceous and some have are rippled. Here, the topmost 10-20 cm of the siltstone contains some rootlets to the overlying G2 coaly member.

- *Member G2 (231.2 m-201.1)*

This member is 30.17 m thick in a particular borehole, consisting of alternating carbonaceous mudstones and thin mixed bright coal beds or lenses. These coals have some siderite and scarce pyrite. Near the top of the member between 201.9m and 201.7, there is 24 cm of limestone with greyish-brown veins and calcitic coaly shale that were encountered. A north northwest- south southeast trending channel-fill with a thickness of up to 5 m, consisting of dark grey mudstone and siltstone with pale medium grained sandstone lenses. These channels only occur in thick Member G2 sequences only, this increase in thickness seems to be gradual and the channels have a non-erosional base. Therefore, these channels are thought to be lacustrine infills which most likely formed in zones of temporarily increased subsidence. There are a couple of thin silty pale mudstone bands within G2 which could be tuff horizons.

- *Member G3 (201.1 m-199.3 m)*

This member consists of a seam coal 1- 2 m thick, known as the Serowe Bright. A pale limestone band 12 cm divides the seam and towards the top, a carbonaceous mudstone 14 cm thick. Though irregular, the limestone band is thought to have originated through similar

processes to the bands in the Morupule Formation, Member F1. Deposition of the Serowe formation occurred in a relatively stable and low energy environment, this this supported by the lateral extent and fine grain size of the lithologies. The presence of fine laminae, ripple bedding and bioturbated beds also suggests slow deposition in a low energy regime. Sideritic nodules are proposed to have formed in shallow water and are common in ancient lake deposits.

Since the silts are reworked and generally borehole sorted, they were probably deposited in a marginal lacustrine deposit spread over swampy plains. Rootlets in G2 coals are indicative of their in situ development and generally, the Serowe coals including G3 have a characteristic sharp contact with their interbedded mudstones. These coals are predominantly bright, indicating a higher proportion of plant matter and less argillaceous material. The Serowe Formation is characteristic of a relatively stable and low energy environment, with the coal deposited in a flat surface of a tectonically stable trough of slow subsidence.

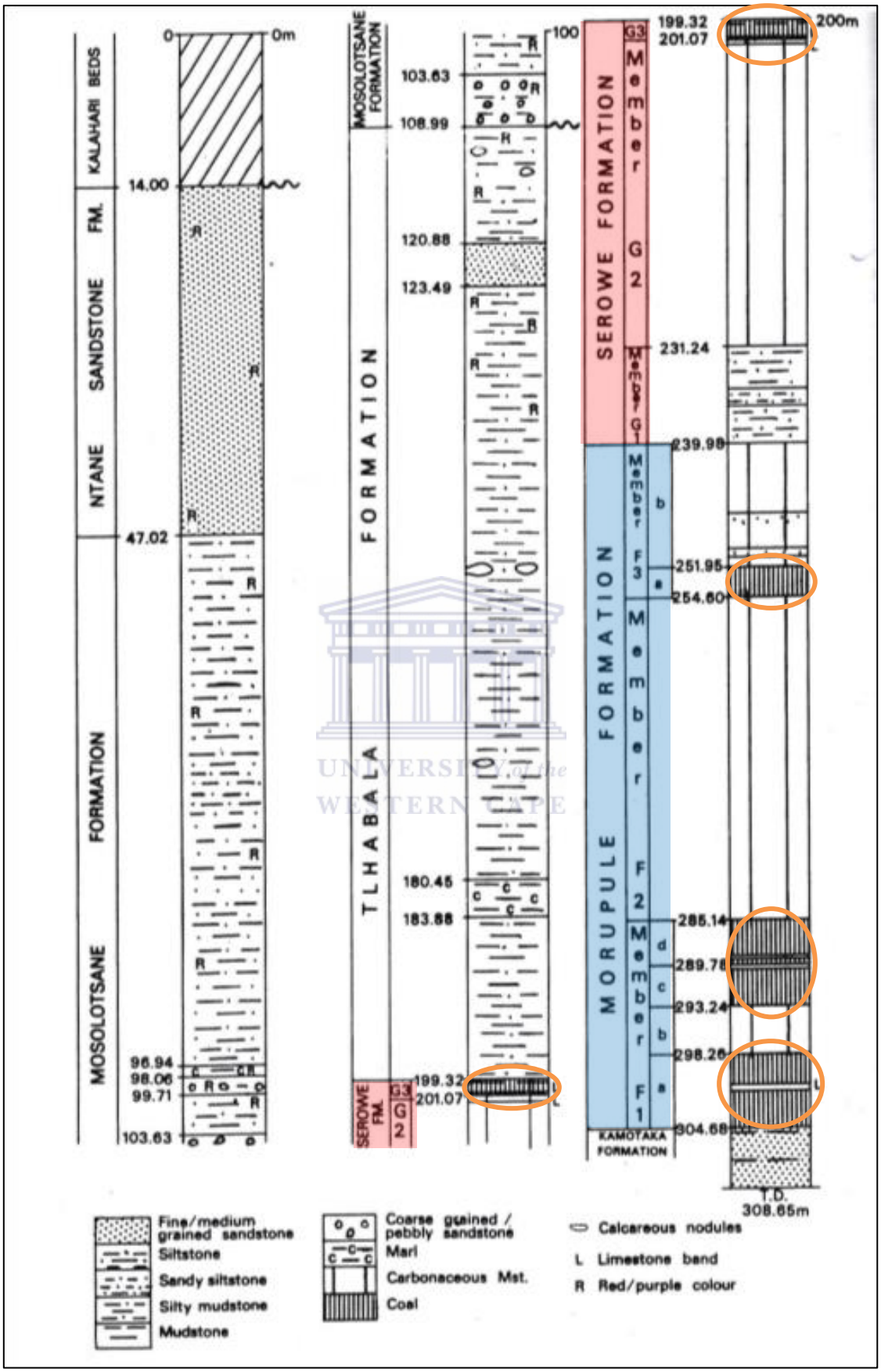

Figure 6: Generalized lithostratigraghy of the south eastern Central Kalahari sub-Basin from borehole C165 (Smith, 1984).

3. Literature Review

3.1 Coal and CBM Generation

Coal is a combustible rock that comprises of more than 50% organic matter by weight. This metamorphosed rock was accumulated by the decomposition and alteration of plant remains forming peat in temperate and tropical swamps and bogs. The process of peatification includes chemical and microbial changes of the organic matter that results in formation of hydrogen-rich humic constituents (Flores et al., 2008). Coalification is the gradual change in physical and chemical properties of peat in response to temperature, pressure and geologic time. The peat transforms to higher ranking lignite, sub-bituminous, bituminous to anthracite coal as shown in Figure 7.

With extreme metamorphism, anthracite changes to meta-anthracite and then graphite. During coalification, diagenesis, catagenesis and metagenesis increase fixed carbon and calorific value, decrease moisture content and volatile matter and ultimately generates natural gas (Flores et al., 2008).

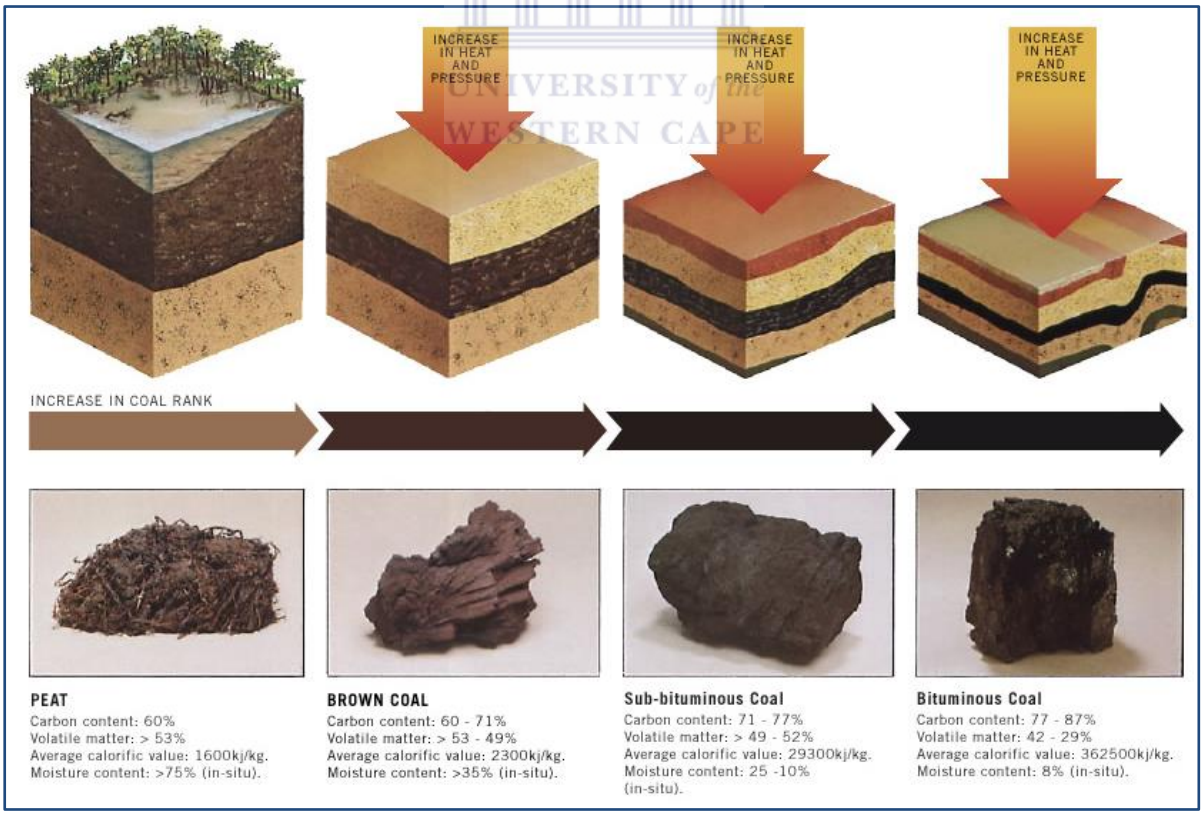

Figure 7: The coalification process with each ranks characteristics listed (Underground Coal, 2011).

Coal bed methane (CBM) is an environmentally friendly natural gas stored in coal seams that has been generated during the process of coalification (Figure 7). CBM occurs within the coal seam as adsorbed gas within the molecular structure of coal, a small amount is stored as free gas in fractures and some in solution with water (Rao et al., 2014). CBM consists of methane and may occur as a mixture of methane, carbon dioxide and water which are the products of coal formation (Rao et al., 2014). The production of methane depends on thickness, rank and maceral composition of coal. CBM can occur as biogenic (microbial) or thermogenic (Figure 8). Commonly, thermogenic gases have been associated with high ranking coal, whereas microbial gases are thought to be produced at early stages of the coalification process (Cokar et al., 2010; Rao et al., 2014).

During the Early Jurassic period, when coal beds of the Kalahari Karoo Basin were at depths of approximately 500 m, dolerite sills and dykes intruded the sedimentary succession. The coal was intruded before it could reach maximum burial depths and thermal maturation (coalification) (Faiz et al., 2013). Adjacent coals were instantly heated, this generated thermogenic gas from the coal. Thermogenic gas generation in coals associated with dolerites was restricted to localised areas around the intrusions. Most of the gas was not adsorbed onto the coal due to extreme temperatures that exceeded 600° C and low pressures at depths of approximately 500 m (Andersen and Potgieter, 2012; Faiz et al., 2013).

The maceral composition of coal seams of the Central Kalahari Karoo Basin may have had a major influence on gas generation potential of the coal (Faiz et al., 2012). It is dominated by vitrinite and inertinite groups with subsidiary quantities of liptinite, however, deeper coals contain less vitrinite and have higher inertinite contents . The coals of the Basin are mainly high ash bituminous in type, have high moisture contents and are of medium calorific value (Bennet, 1989; Faiz et al., 2012).

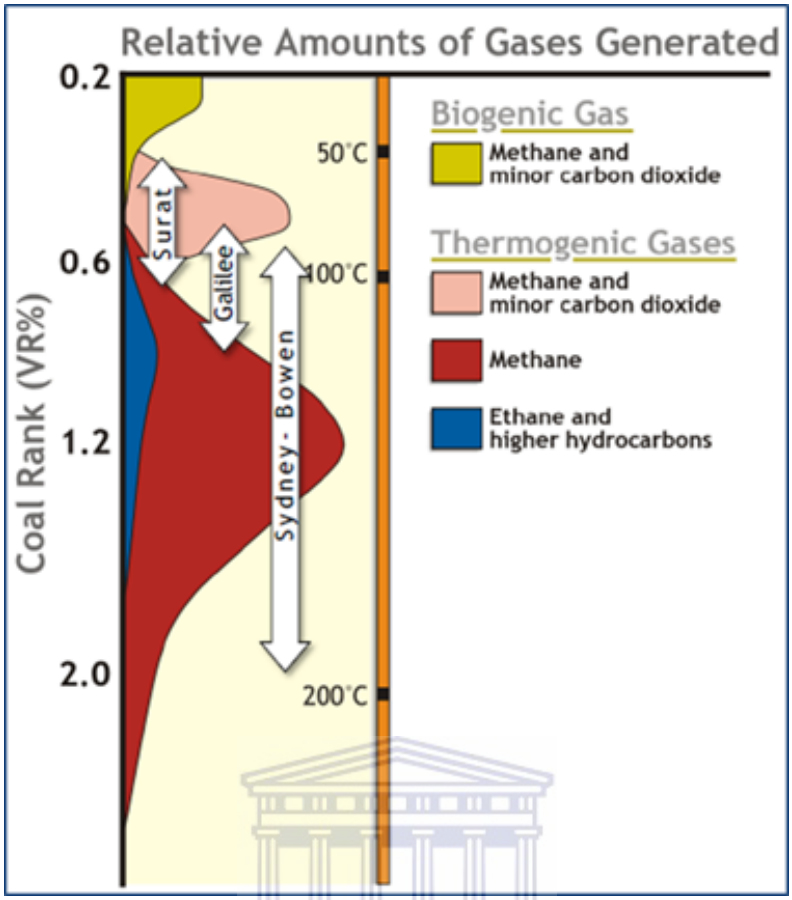

Figure 8: Relative amounts of gas generated as determined by vitrinite reflectance of coal from various basins (Faiz et al., 2012).

3.2 Passey's ΔLogR Technique

Passey et al. (1990) developed a technique used to identify and calculate %TOC in organic matter enriched rocks. This method involves the overlaying of a properly scaled porosity log on a deep resistivity curve. Sonic logs are commonly used as the porosity indicator. However the density logs can be implemented as an alternative. The sonic log is aligned on top of the logarithmically scaled resistivity curve, this is normally indicated where 50 µsec/ft is equal to 1 log decade ohm-m but can also vary. The result is an overlay of the sonic and the resistivity curve in non-source shale (Figure 9). These shale units are characterised by low resistivity readings and are highly unlikely to be gas bearing shale units (Passey et al., 1990; Shiri et al., 2013). Sonic and resistivity log readings in the low resistivity shale are referred to as the baseline readings. These readings will vary with depth of burial and geologic age. This technique assumes that the baseline condition will occur at the non-source interval (Passey et al., 1990; Charsky and Herron, 2013; Sun et al., 2013).

Shale with a source rock potential will display a significant crossover between the two curves; this is termed the ΔLogR separation. The theory behind the crossover is that the presence of organic matter affects the bulk density of a rock and therefore its porosity measurement. The porosity curve detects the low velocity and low density organic matter. The resistivity curve responds to the fluid within the formation, wherein water will yield low resistivity values and hydrocarbons will be highly resistive. Therefore, in organic enriched intervals or hydrocarbon reservoirs, the two curves will separate. A relationship between abundance of organic matter and its maturity is established based on the magnitude of the separation between these curves (Passey et al., 1990; Charsky and Herron, 2013).

Passey et al. (1990) also warn that an anomalous ΔLogR separation not attributed to source rock intervals generally can be a result of hydrocarbon reservoirs, uncompacted sediments, poor borehole conditions, low porosity intervals, evaporates or volcanic rocks. The use of all other wireline logs is emphasized for detection of various lithology properties. In Figure 9, zones A and C display separations between the resistivity and sonic curves. Zone A is a hydrocarbon reservoir and the separation occurs as a result of hydrocarbon detection by the resistivity curve. Low gamma ray readings are used to differentiate these reservoirs from source rock intervals. However, reservoirs which consist of feldspar or mica-rich sandstones may display high gamma ray readings. The absence of longer transit times in their separation reveals the absence of organic matter (Passey et al., 1990).

In mature intervals (zone C) the separation is characterized a response from both curves with resistivity increasing to the right due to the presence of generated hydrocarbons and transit time responding to the low velocity organic matter thereby increasing to the left, this is the ΔLogR separation (Figure 9). Non-source shaly intervals (zone B) are characterized by the two curves overlying each other (Passey et al., 1990; Shiri et al., 2013).

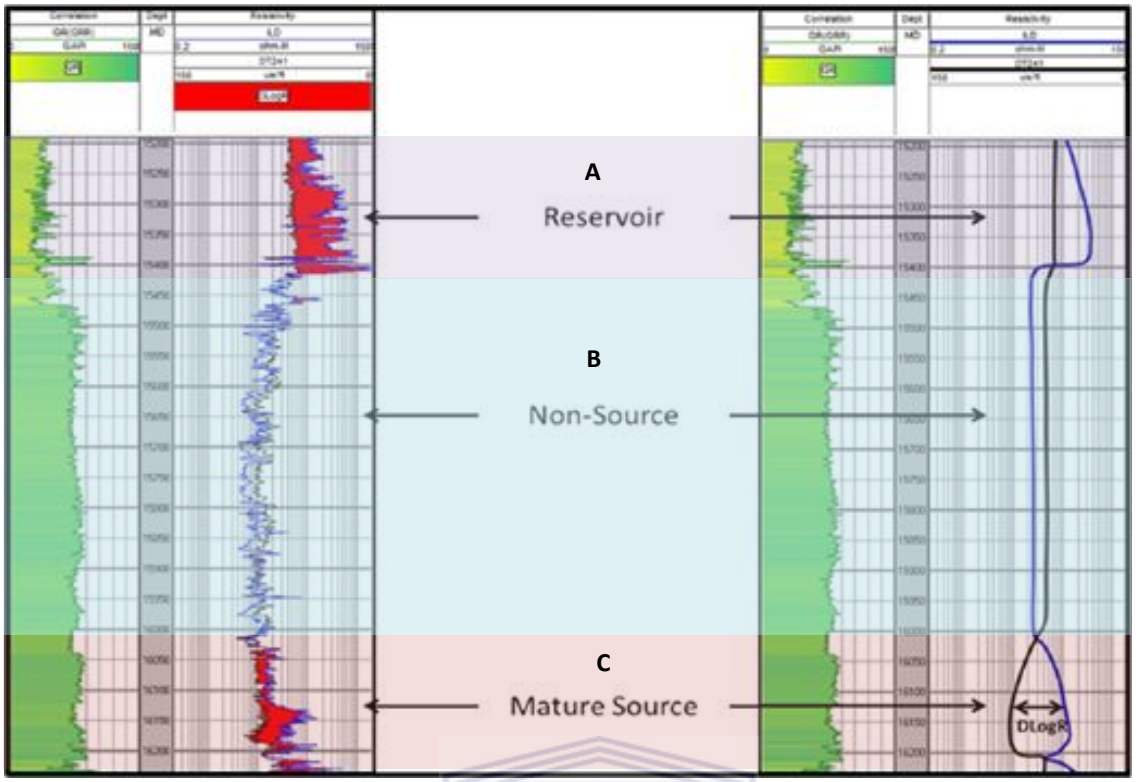

Figure 9: Actual (left) and theoretical (right) resistivity-sonic overlay responses in reservoir, non-source (organic-lean) and mature source (After Berch, 2013).

For empirical calculations, equations 1 or 2 are used (after Passey et al., 1990; Crain, 2013):

*SlogR = log (RESD / RESDbase) + 0.02 * (DTC – DTCbase)…. (1)*
*DlogR = log (RESD / RESDbase) – 2.5 * (DENS – DENSbase)…. (2)*
Where:
SlogR, DlogR= Passey's number from sonic, density (fractional)
RESD = Deep resistivity in any zone (ohm-m)
RESDbase = Deep resistivity baseline in non-source rock (ohm-m)
DTC = Compressional; sonic log reading in any zone (usec/ft)
DTCbase = Sonic baseline in non-source rock (usec/ft)
DENS = Density log reading in any zone (gm/cc)
DENSbase = Density in non-source rock (gm/cc).

Then, the percentage of TOC can be determined from equations 3 or 4; provided the level of organic metamorphism (LOM) is known:

*TOCs = SlogR * 10^ (0.297 – 0.1688 * LOM)…. (3)*
*TOCd = DlogR * 10^ (0.297 – 0.1688 * LOM)…. (4)*
Where:
LOM = Level of organic metamorphism (unitless)
TOCs, d = Total organic carbon from Passey's method (weight fraction)

Finally, calculated TOCs or TOCd is then compared to measured core organic carbon and the strength of correlation of their relationship is assessed. Using the ΔLogR method does not require any calibration to the core data for comparison.

3.3 Thermal Maturity

The primary factor that determines if a source rock can produce any hydrocarbons is thermal maturity (Shiri et al., 2013). Vitrinite reflectance (%Ro) is the most commonly used maturation indicator of organic matter in sedimentary rocks. Vitrinite is a coal maceral found in humic coals, as coaly inclusions in shales and mostly disseminated in other sedimentary rocks. This reason justifies the direct application of vitrinite reflectance in studying temperature histories of petroleum source rocks. Vitrinite reflectance is evaluated by the measurement of light reflected from vitrinite particles within a sedimentary rock. The more light reflected indicates a more mature source rock sample (Hood et al., 1975; Berch, 2013).

A method developed by Hood et al. (1975) for quantifying thermal maturity, which directly correlates to vitrinite reflectance, is the "level of organic metamorphism" (LOM). LOM is a scale that describes the degree of thermal metamorphism of organic matter with burial and is based on coal rank (Hood et al., 1975). Temperature controls the conversion of kerogen to hydrocarbon molecules. The effects of organic metamorphism are the changes in the physical and chemical properties of kerogen (Hood et al., 1975). The coal rank scale has provided the basic framework in studying the process of coalification. This is used effectively in comparing LOM stages in petroleum generating source rocks as shown in Figure 10. The scale covers the entire range from the onset of petroleum generation to its destruction (Hood et al., 1975).

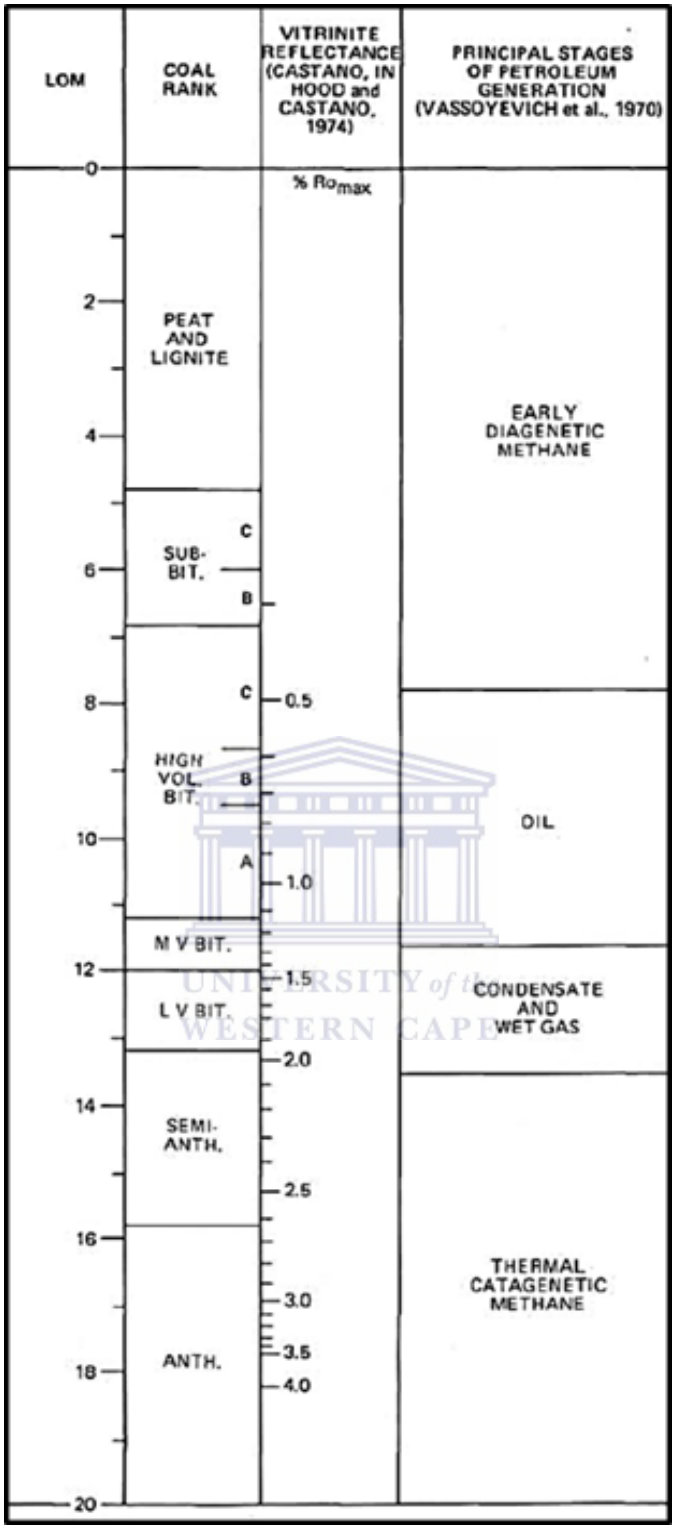

Figure 10: Scale relating coal rank, vitrinite reflectance (%Ro) and petroleum generation stage to LOM. LOM is unitless (Hood et al., 1975).

3.4 Total Organic Carbon (TOC)

Total organic carbon (TOC) is a measurement of the organic richness in a given sedimentary rock reported in weight percent of organic carbon. Derived from organic matter, organic carbon is the component of the rock sample that can potentially convert to hydrocarbons (Jarvie, 1991). TOC analysis is usually the first screening process done to assess potential for hydrocarbon generation. As indicated in Figure 11, organic carbon only takes up a small fraction in a volume of sediment sample (typically shale). A TOC value of 1 wt % implies that in 100 grams of sediment, only 1 gram organic carbon exists (Jarvie, 1991). However, coal generally contains greater than 50 wt% and 70% by volume of TOC (Rice, 1993).

A TOC percentage comprises three carbon components: extractible organic matter carbon (EOM carbon), convertible carbon and a portion residual carbon (Figure 9) (Jarvie, 1991).

- The EOM carbon is extractable hydrocarbons trapped in rock pore spaces. It is formed as a result of thermal cracking of kerogen and biological markers that are directly incorporated EOM carbon is typically less than 1% of the bulk TOC in shales,
- Convertible carbon is carbon found in kerogen, it is essentially the TOC component that has the potential to generate hydrocarbons, and
- Residual carbon is also a component of kerogen but has no hydrocarbon generating potential due to its hydrogen-deficient and condensed chemical structure (Jarvie, 1991; Berch, 2013).

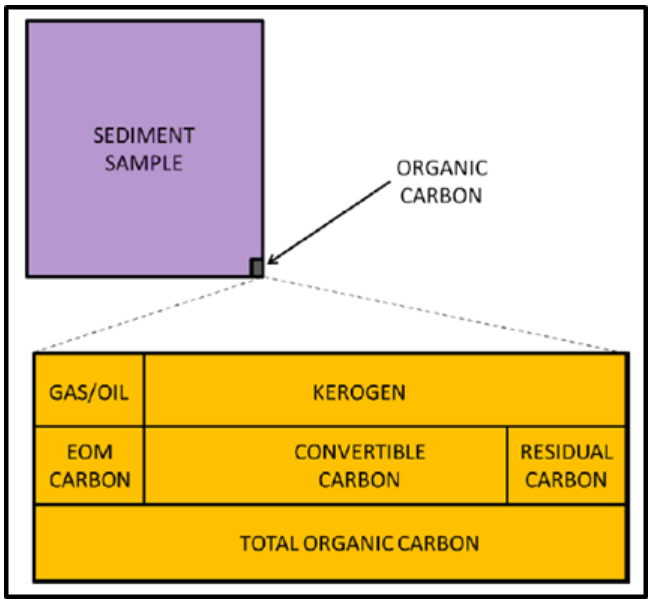

Figure 11: An illustration of organic carbon distribution in a given sediment sample (Berch, 2013).

4. Data and Methods

4.1 Geological Logs

Core log descriptions provided by Kubu Energy were used to substantiate the various lithology interpreted using wireline logs. Various structures, mineralogy and coal types, were described in detail within each formation, with visible burnt (devolatised) samples noted as borehole.

4.2 Wireline Logs

Andersen Geological Consulting conducted the geophysical logging of exploration boreholes (CH1-CH9). Wireline logs were provided for all 9 boreholes, they included gamma ray (CDEN_00: GAMMA), density (CDEN_00: DENCDL), resistivity (ELOG_00: LATERAL) and sonic logs (FWFS_00: DELTAT). These logs were important in identifying lithologies.

4.2.1 Wireline log uses

- The gamma ray log measures the level of natural radioactivity in the rock formation. Sands generally display low gamma ray responses whilst shaly rocks display a high response as they are enriched with uranium, thorium and potassium
- The density log is the main porosity measuring tool. It measures the bulk density of the rock including the rock matrix and the fluid contained within pores
- The sonic tool measures the transit time taken to pass through a formation, therefore it is also used to determine the porosity of that formation. Sound waves travel in a high-density (low porosity) formation faster than in a low-density (high porosity) formation
- Resistivity tools measure the electrical resistivity of rocks which indicates the presence of hydrocarbons. Rocks saturated with water display a low-resistivity, while those saturated with oil or gas respond with a high resistivity.

4.2.2 Wireline log application

Histogram distributions of gamma ray, density, sonic and resistivity log measurements were useful in classifying rock types. For example, a histogram distribution of gamma ray logs for all boreholes (Figure 12) was used to determine ranges for gamma ray measurements in order to classify lithology types based on clay content. The mean gamma ray value, which is 113.27, was used as a cut off value for differentiation. Below 113.27 °API, lithologies were

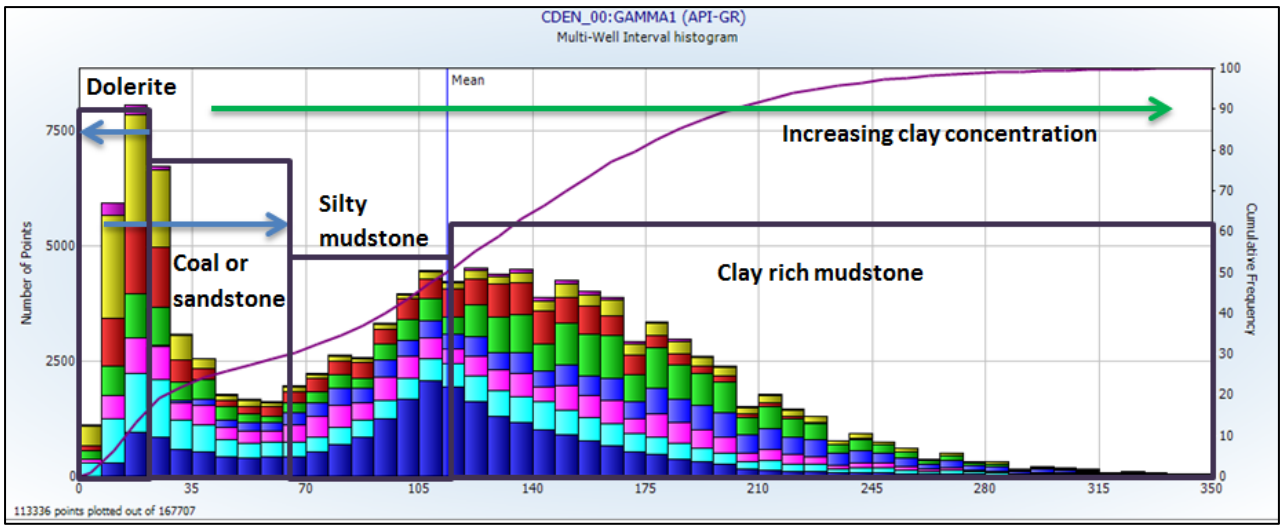

Figure 12: Histogram distribution of clay content in all boreholes using gamma ray curves.

identified as dolerite, coal or sandstone or silty mudstone. Above 113.27 °API, the lithology was considered as clay enriched mudstone. The density log distribution histogram served to segregate intervals with gamma ray values less than 113.27° API into dolerite, coal or silty mudstone. Table 1 shows log measurement ranges used to characterize lithology types.

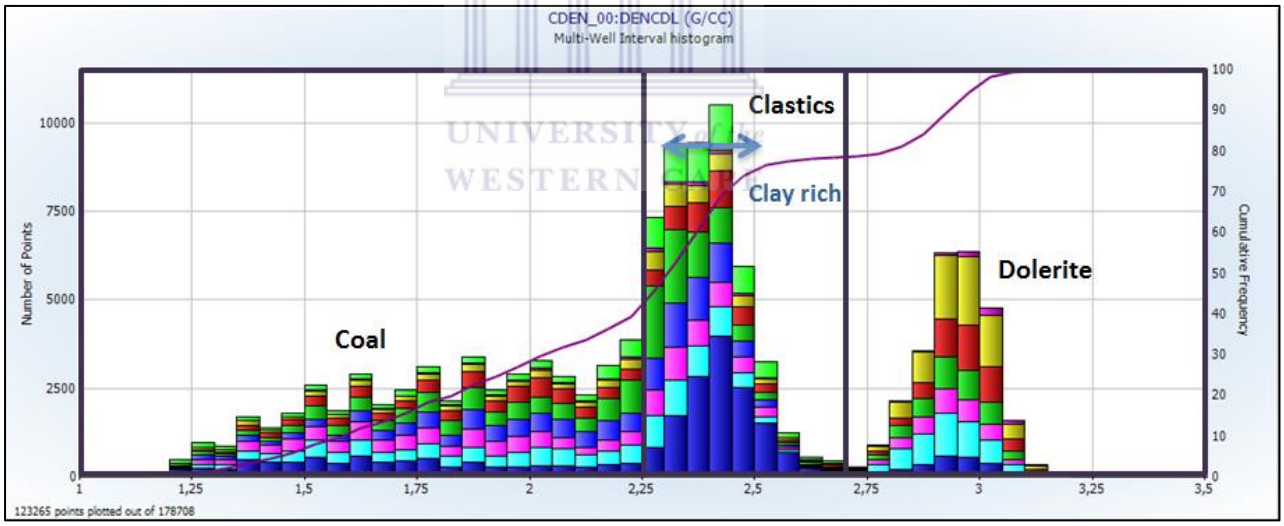

Figure 13: Distribution of lithology densities in all boreholes. Density range of clay rich mudstone overlaps with that of sandstone-siltstone clastic mix.

Lithology	Gamma ray (°API)	Density (g/cc)	Resistivity (ohm-m)	Sonic (µsec/m)
Dolerite	3 - 21	2.7- 3.2	110-1000	50- 180
Coal	6 - 65	1.12- 2.25	18- 110	280- 480
Silty to Quartz rich clastics	65-113	2.25- 2.7	0.1- 5	180- 250
Clay rich	113- 336	2.3- 2.5	5- 20	250- 320

Table 1: Approximate log measurement ranges used to characterize lithology types.

Resistivity and transit time histogram distributions are provided in Appendix A. Resistivity tends to be higher and transit time slower in coal (Figure 14) as a result of the gas contained within its pores. Dolerite intrusions are characteristic of resistivity measurements even higher than that in coal and fastest transit time.

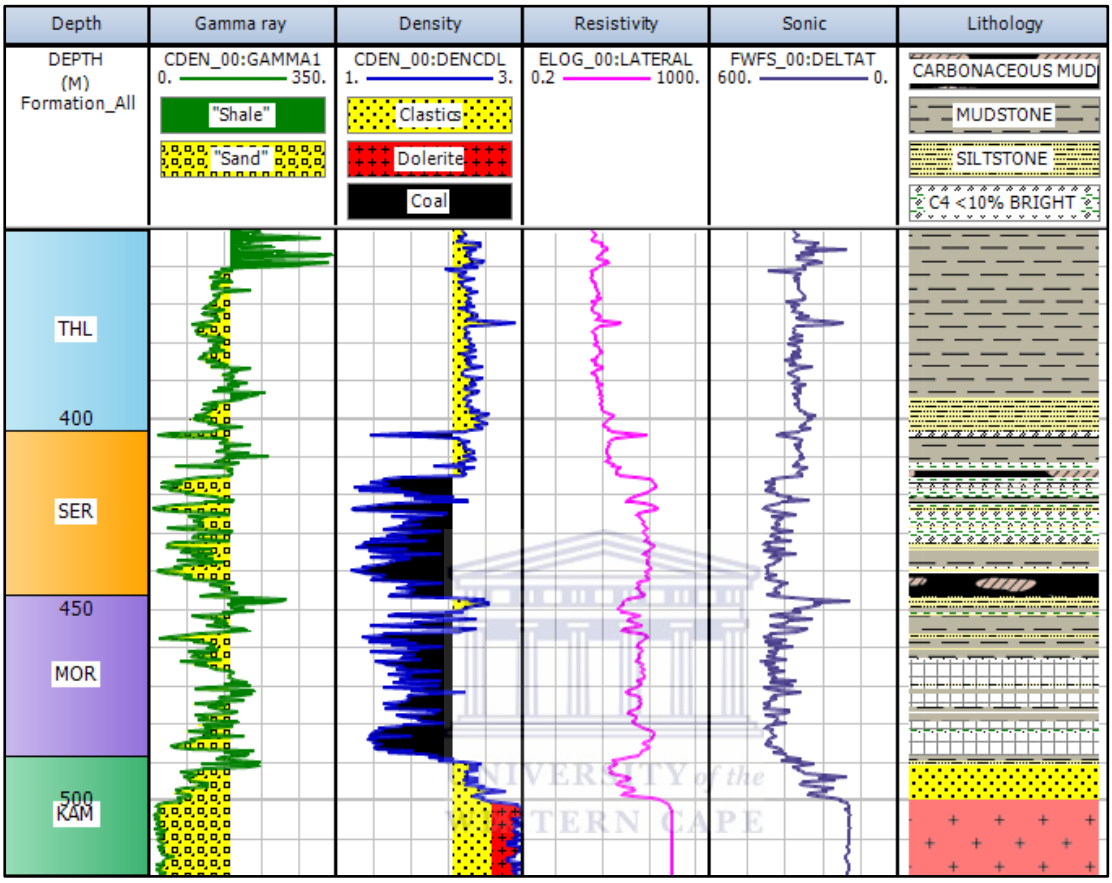

Figure 14: An example of a log suite display from borehole CH7. Coal was identified by its low gamma ray values, low density, high resistivity and slower transit time.

4.3 Proximate Analysis

Proximate analysis measures in the laboratory the proportion of fixed carbon, ash, volatile matter and moisture in coal. These proportions are reported as weight percentages. Analysis of the coal samples was conducted by Weatherford Laboratories according to the Australian Standard for coal analysis and testing, AS 1038.3-1989 (Standards Association of Australia, 2000a). The procedure involves drying a known mass of coal in an oxygen-free (nitrogen flush) oven at 105-110°C for a period of 1.5 to 3 hours. After removal from the oven, and subsequent to the sample being placed in a desiccator, the coal was weighed, and the loss of mass ascribed to inherent moisture.

The sample is then heated in a cylindrical silica crucible in a muffle furnace at 900°C for seven minutes. The loss of mass recorded during this process is equal to the proportion of

volatile matter present in the sample. Determination of ash content is achieved by combusting the coal until a constant mass is attained by heating the sample to 500°C for 30 minutes before increasing the temperature to 815°C, until combustion is complete. The ash percentage is calculated from the mass of the residue remaining after incineration. The amount of fixed carbon was not determined directly, but was inferred from the difference between the sums of all other components.

4.4 Thermal Maturity: Vitrinite Reflectance

Vitrinite reflectance (%Ro) measurements were also conducted by Weatherford Laboratories according to the Australian Standard for microscopical determination of the reflectance of coal macerals, AS2456.3 (Standards Association of Australia, 2000b). The percentage of light reflected from the vitrinite maceral was calibrated against a material with a known reflectivity value expressed in percent. A minimum of fifty (50) readings were measured for each sample to have a precise mean maximum reflectance value. Also, thermally affected samples were noted in the report. %Ro measurements were then used to classify samples as immature, mature or post-mature (Table 2).

Phase	Ro (%)
Immature	< 0.6
Oil	0.6- 1.1
Wet Gas	1.1- 1.4
Dry Gas	1.4- 4.0
Post-mature	> 4.0

Table 2: Phases of petroleum generation with their corresponding vitrinite reflectance indices (Standards Association of Australia, 2000b).

Passey's ΔLogR method requires knowledge of an LOM value in order to convert the ΔLogR separation to a quantitative %TOC. In order to determine LOM values from %Ro measurements, maturity ranges provided by Hood et al. (1975) in Figure 10 were used. A mathematical relationship (Figure 15) was established in Microsoft Excel by crossplotting the LOM with %Ro to determine the regression equation below:

$$LOM = 0.004\,(\%Ro^3) - 0.4987\,(\%Ro^2) + 5.1115\,(\%Ro) + 5.5714 \ldots (5)$$

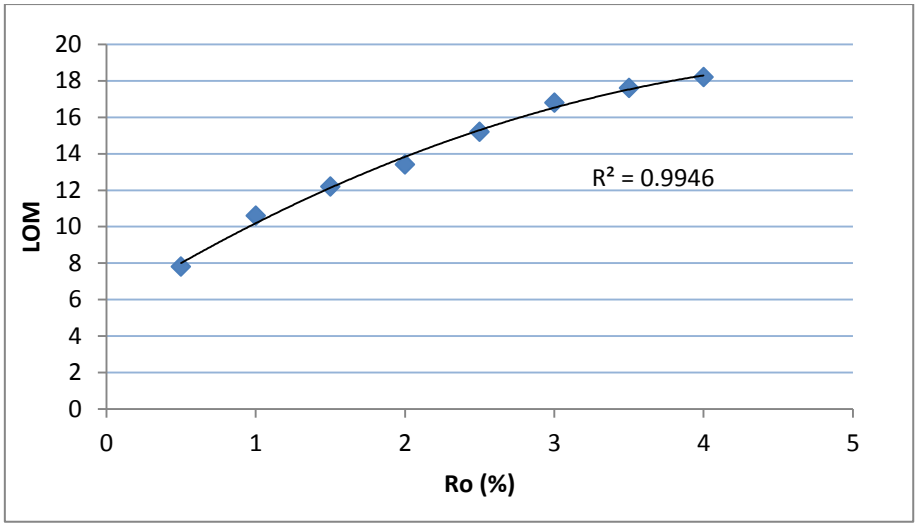

Figure 15: Graphical representation of the relationship between %Ro and LOM.

Using the relationship established in Figure 15, Table 3 was created in order to assign %Ro measurements their corresponding LOM values. Based on the established correlation, an LOM value less than 8.46 correlates to thermally immature coal, and LOM values ranging from 8.46- 10.59, 10.59-11.76, and greater than 11.76 correlate to the oil window, the wet gas/condensate window, and the dry gas window.

Coal Rank	Ro (%)	LOM
Peat	< 0.23	< 6.72
Lignite	0.23- 0.36	6.72- 7.35
Sub-bituminous: C	0.36- 0.41	7.35- 7.58
Sub-bituminous: B	0.41- 0.47	7.58- 7.86
Sub-bituminous: A	0.47- 0.49	7.86- 7.96
High-Volatile Bituminous: C	0.49- 0.51	7.96- 8.05
High-Volatile Bituminous: B	0.51- 0.69	8.05- 8.86
High-Volatile Bituminous: A	0.69- 1.11	8.86- 10.64
Medium-Volatile Bituminous	1.11- 1.6	10.64- 12.49
Low-Volatile Bituminous	1.6- 2.04	12.49- 13.96
Semi-Anthracite	2.04- 2.4	13.96- 15.02
Anthracite	2.4- 5	15.02- 19.16
Meta-Anthracite	> 5	> 19.16

Table 3: A quantitative relationship between coal rank, %Ro and LOM.

4.5 Passey's method Input Parameters

For DlogR/SlogR calculations, spreadsheet listings from each borehole with deep resistivity (RESD), density (DENS) and sonic (DTC) measurements every 0.01m were exported from Interactive Petrophysics (IP) into excel where only values for the sampled interval points were extracted as shown in Figure 16 below.

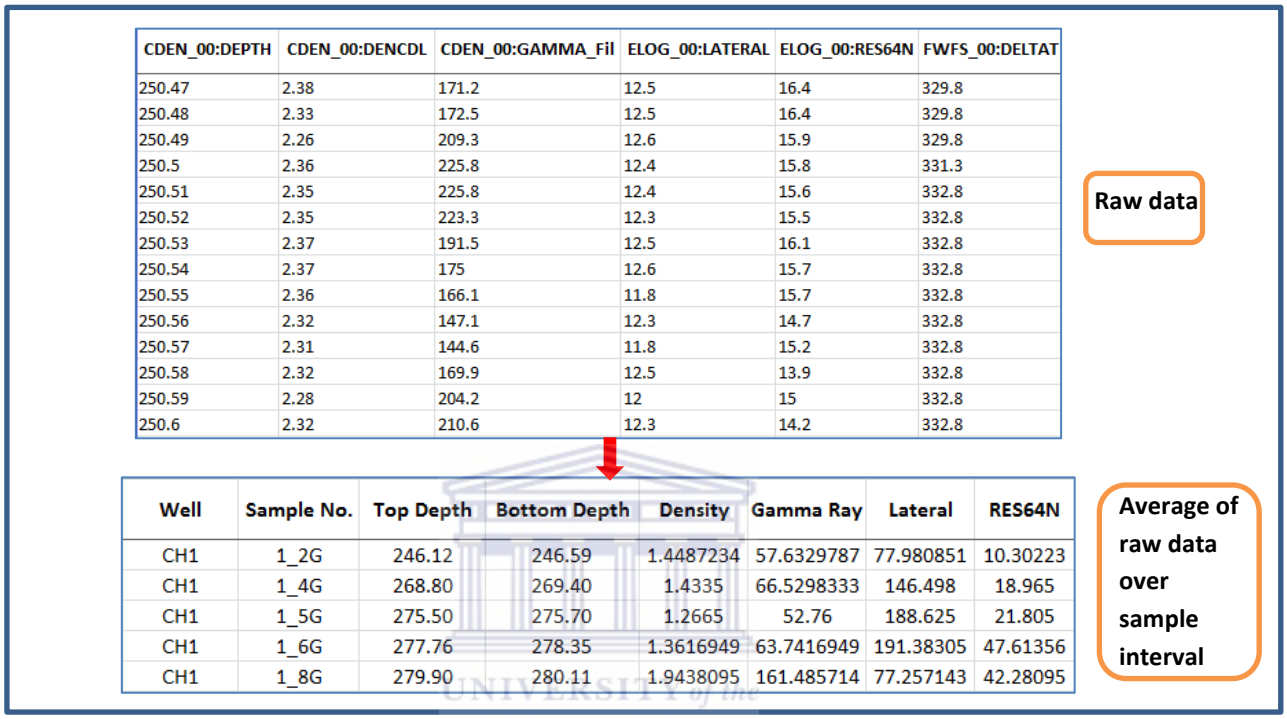

CDEN_00:DEPTH	CDEN_00:DENCDL	CDEN_00:GAMMA_Fil	ELOG_00:LATERAL	ELOG_00:RES64N	FWFS_00:DELTAT
250.47	2.38	171.2	12.5	16.4	329.8
250.48	2.33	172.5	12.5	16.4	329.8
250.49	2.26	209.3	12.6	15.9	329.8
250.5	2.36	225.8	12.4	15.8	331.3
250.51	2.35	225.8	12.4	15.6	332.8
250.52	2.35	223.3	12.3	15.5	332.8
250.53	2.37	191.5	12.5	16.1	332.8
250.54	2.37	175	12.6	15.7	332.8
250.55	2.36	166.1	11.8	15.7	332.8
250.56	2.32	147.1	12.3	14.7	332.8
250.57	2.31	144.6	11.8	15.2	332.8
250.58	2.32	169.9	12.5	13.9	332.8
250.59	2.28	204.2	12	15	332.8
250.6	2.32	210.6	12.3	14.2	332.8

Raw data

Well	Sample No.	Top Depth	Bottom Depth	Density	Gamma Ray	Lateral	RES64N
CH1	1_2G	246.12	246.59	1.4487234	57.6329787	77.980851	10.30223
CH1	1_4G	268.80	269.40	1.4335	66.5298333	146.498	18.965
CH1	1_5G	275.50	275.70	1.2665	52.76	188.625	21.805
CH1	1_6G	277.76	278.35	1.3616949	63.7416949	191.38305	47.61356
CH1	1_8G	279.90	280.11	1.9438095	161.485714	77.257143	42.28095

Average of raw data over sample interval

Figure 16: An example from borehole CH3 showing Inputs for DlogR/SlogR equations extracted from IP for sampled coal intervals. Raw data averages for sampled intervals in all boreholes are provided in Appendix E.

RESDbase, DENSbase and DTCbase are the deep resistivity, density and transit time readings respectively, from the baseline interval as discussed in section 3.2. These were read off logs directly in baseline intervals after scaling of the deep resistivity lateral log with the sonic and density logs (Figure 17). Both the sonic and density logs coupled with resistivity were used to achieve DlogR and SlogR separations. These separations were quantified and then used together with individual LOM values as inputs in the TOCd and TOCs calculations in Microsoft Excel. RESDbase, DENSbase and DTCbase readings for all boreholes are provided in Appendix B. For the generation of TOC curves in IP Software, the same inputs were used but instead of inserting raw data averages from spreadsheet listings in the equation, actual resistivity, density and sonic curves were used rather.

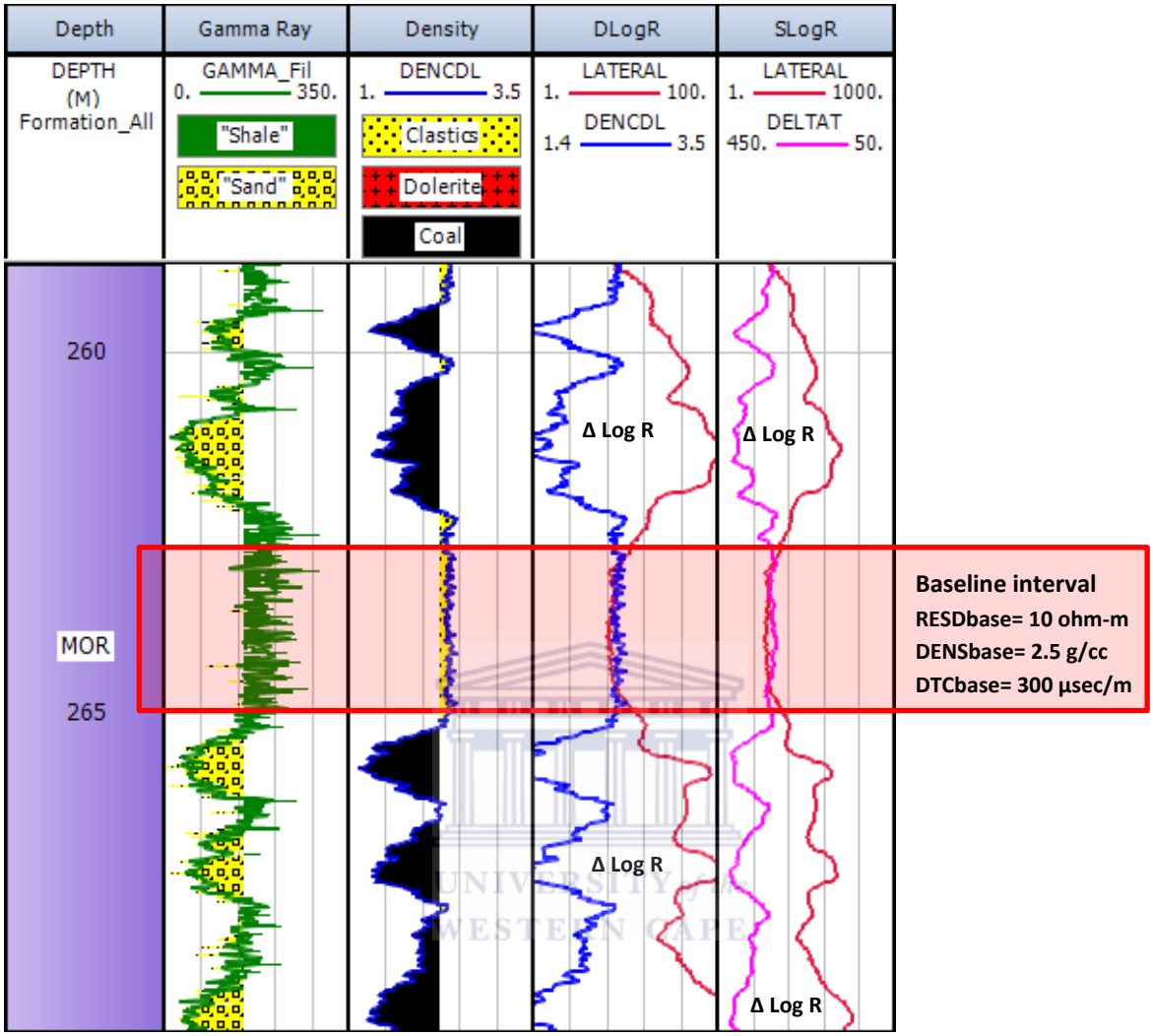

Figure 17: An example from borehole CH1 showing ΔLogR separation intervals from both porosity curves and a shale baseline interval with RESDbase, DENSbase and DTCbase readings.

5. Results and Discussions

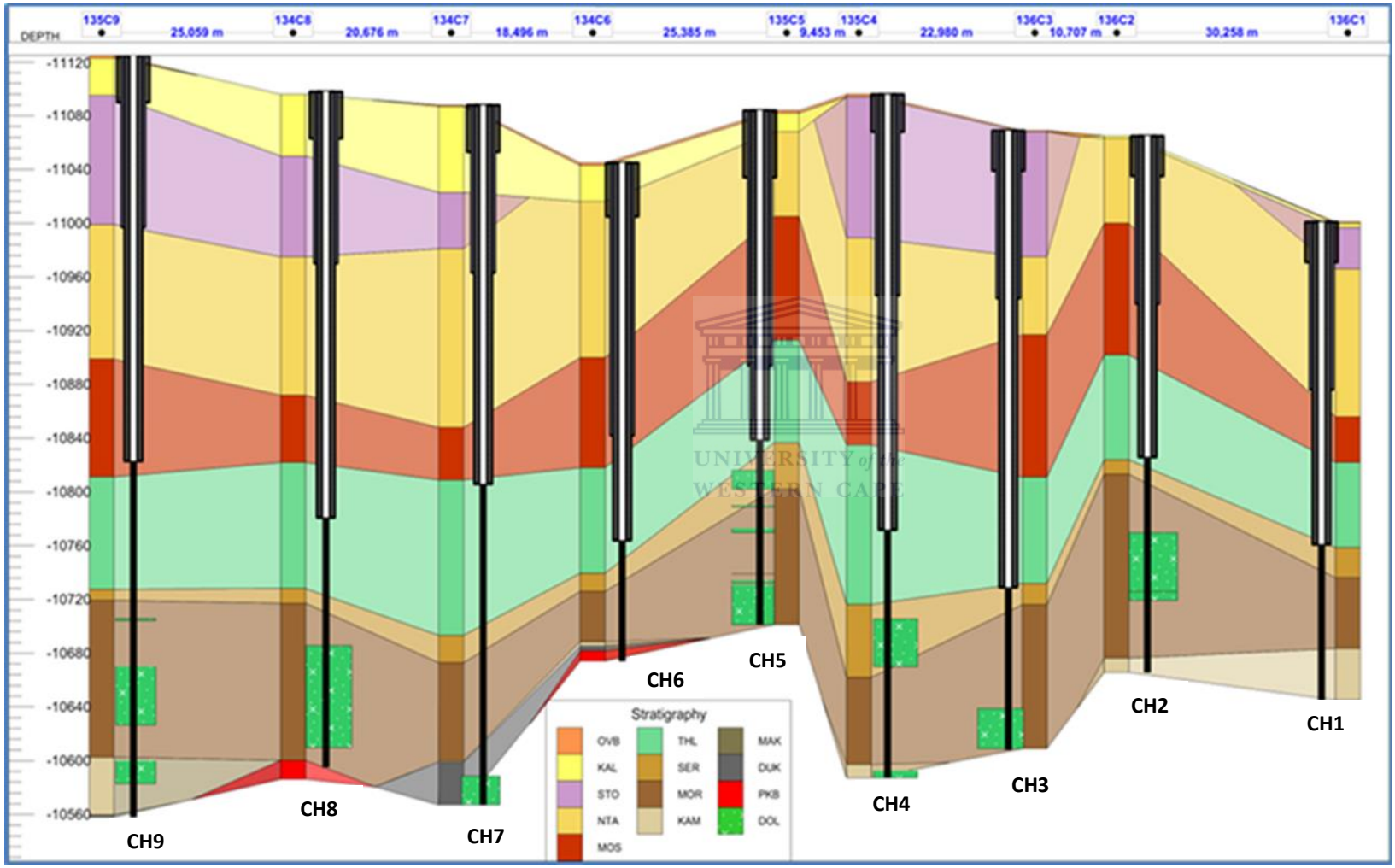

Figure 18: Cross-section through boreholes CH1 to CH9 showing stratigraphic boundaries and dolerite intrusions. Formation abbreviations: OVB- Overburden, KAL- Kalahari , STO- Stormberg , NTA- Ntane , MOS- Mosolotsane, THL- Tlhabala , SER- Serowe , MOR- Morupule, KAM- Kamotaka, MAK- Makoro, DUK- Dukwi, PKB- Pre Karoo Basement and DOL- Dolerite intrusion (Sill) (Roon and Parker, 2014).

5.1 Thermal Maturity

The Mean maximum %Ro for all samples analysed indicates that there is a wide distribution of measurements, ranging from 0.4% to 5.53% (Figure 19a). As shown in the stratigraphic model in Figure 18, boreholes CH1 and CH6 did not intercept dolerite intrusions and appear to have not been thermally affected at all. Therefore, %Ro measurements in these boreholes are assumed to have been attained due to normal geothermal gradients in the basin. The geothermal gradient in the basin is approximately 36°C/km (Haddon, 2005). %Ro measurements in CH1 and CH6 are between 0.44% and 0.65% indicating that coal in both boreholes is mostly immature to marginally mature for any significant thermogenic gas generation. Also, %Ro increases with depth (Figure 19a) in these boreholes, signifying the role played by burial metamorphism. These boreholes can be used for control and comparison of %Ro in boreholes affected by intrusions.

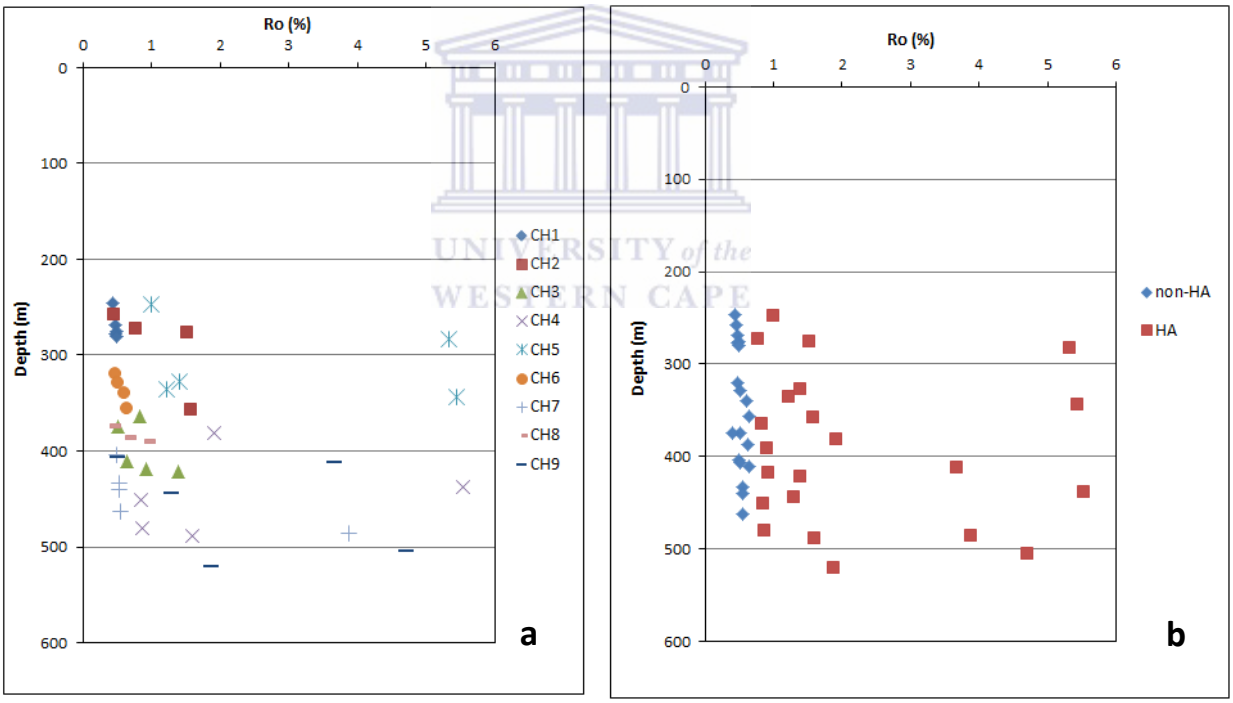

Figure 19: a. Vitrinite reflectance (%Ro) distribution with depth for all boreholes. b. %Ro trends with depth for coals heat affected (HA) by dolerite intrusions and non-heat affected (non-HA) coals.

In boreholes CH2, CH3, CH4, CH5, CH7, CH8 and CH9 some coal intervals are noted in both vitrinite reflectance analysis reports and core descriptions as having been affected by the relative instantaneous heating from the intrusions. This is evident in their %Ro measurements ranging between 0.77% and 5.53% (Figure 19b). Coals in closest contact with intrusions show %Ro> 5% which rapidly decreases to 0.77% with increasing distance from

the intrusion. This rapid decrease in %Ro suggests that the contact metamorphism of intrusive events was probably confined to a few meters on either side of intrusion. This is supported by Golab (2003) and Jiang et al. (2011) who both state that during an igneous intrusion, the alteration of coal is highest at the contact and extends into the coal as an aureole. The aureole size depends on the rank, petrology, thermal conductivity, fissure development and cleats, water content, temperature and pressure of the coal as borehole as the chemistry, temperature, degree of intrusion crystallization and the nature of volatile fluids (Golab, 2003).

In his study, Bennet (1989) found that coals of the Mmamabula area in the Central Kalahari Karoo Basin obtained mean maximum %Ro of between 0.52 and 0.64%. He attributed the immaturity of the coals to generally limited basin subsidence and burial depths. %Ro measurements from his study are consistent with those of CH1 and CH6, which measured between 0.44 and 0.65 %Ro. Evidenced by boreholes CH1 and CH6, the %Ro indicates that coals in the basin are primarily sub-bituminous type B to high volatile bituminous type B in rank. Higher ranking volatile bituminous to anthracitic coals formed by rapid heating which occurred in localised areas adjacent to intrusions. In Figure 20, samples D12 and D13 of borehole CH3 have not thermally metamorphosed whereas intervals above and below them have been affected. Clearly, heat effects were dependant on the extent of the contact aureole for each sill.

Well	Formation	Sample No.	Top Depth (m)	Bottom Depth (m)	Ro (%)	Coal Rank	LOM	Maturity Phase
CH3	Serowe	D5	364.37	364.67	0.83	High- Volatile Bituminous: A	9.47	Mature
CH3	Serowe	D12	374.10	374.70	0.52	High- Volatile Bituminous: B	8.10	Immature
CH3	Serowe	D13	410.25	410.48	0.64	High- Volatile Bituminous: B	8.64	Mature
CH3	Serowe	D16	418.44	419.04	0.92	High- Volatile Bituminous: A	9.85	Mature
CH3	Serowe	D18	421.46	422.06	1.39	Medium- Volatile Bituminous	11.72	Mature
DOLERITE: 431.7-460.7 m								

Figure 20: Higher ranking metamorphosed coals with less mature intervals between them. Heat affected samples are highlighted in yellow. Dolerite intervals are denoted in blue. Appendix C tabulates LOM, rank and maturity phase of all samples.

Based on sample %Ro measurements and distance between coal intervals and sill in each borehole, the sill intrusion area can be divided into three zones: (1) contact metamorphism zone which is within 2- 12m from the sill, (2) thermal evolution zone which is within distances of 12- 54 m from the sill and (3) unaltered zone. The contact metamorphism zone

displays %Ro from 3.67% up to 5.53%; the thermal evolution zone %Ro ranges between 0.77% and 1.91%. The unaltered zone is characterised by %Ro of between 0.44% and 0.65%.

LOM was calculated using equation:

$$LOM = 0.004 (\%Ro^3) - 0.4987 (\%Ro^2) + 5.1115 (\%Ro) + 5.5714 \ldots. (5)$$

Since LOM values are determined based on %Ro measurements, they display similar trends as %Ro (Figure 19). Heat affected samples are mostly mature covering the oil, wet gas and condensate and dry gas windows with a few that are post mature. Their LOM ranges from 9.21 to 19.26 with post-mature samples yielding values greater than 18.29. It is clear that the LOM of these coals was accelerated by heat effects. Non-heat affected samples from all boreholes show LOM values ranging from 7.72 to 8.68, these are considered immature. Corresponding LOM values in terms of the three zones of the intrusion area are 7.72- 8.68, 9.21- 13.54 and > 17.81 for the unaltered, thermal evolution and contact metamorphism zones respectively (Figure 21).

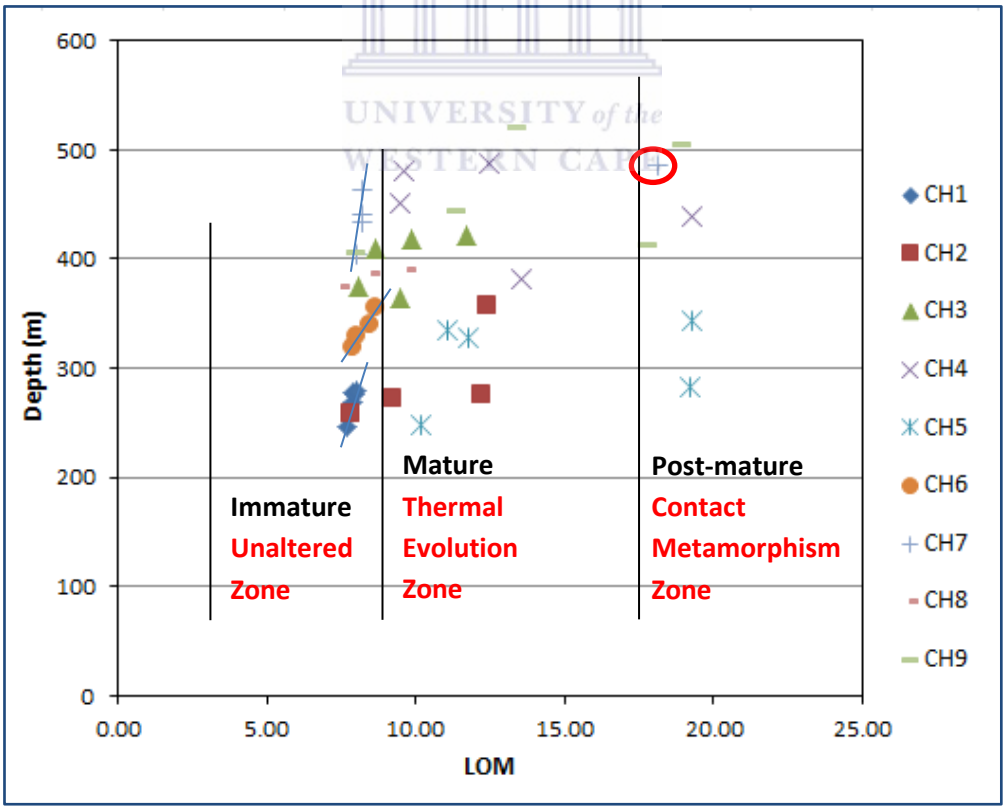

Figure 21: Relationship between LOM and depth in all boreholes. The three zones of the intrusion area are delineated. Unintruded CH1 and CH6 display an increase in LOM with depth trend, CH7 shows a similar trend except for one sample that is heat affected (encircled in red).

Similarly with %Ro, boreholes CH1 and CH6 display increasing LOM and rank with depth. In intruded boreholes CH2 and CH8 (Figure 22) there is an increase of LOM with depth probably due to the fact that sill intrusions in both boreholes only occur adjacent to deeper sampled intervals. Therefore alteration was only experienced in these intervals governed by aureole dynamics where the coals in contact or adjacent to the intrusion will be heated the most. The intrusions have altered the relationship between maturity and depth in boreholes CH3, CH4, CH5 and CH9.

Well	Formation	Sample No.	Top Depth (m)	Bottom Depth (m)	Ro (%)	Coal Rank	LOM	Maturity Phase
CH2	Serowe	D3	257.99	258.60	0.46	Sub- Bituminous- B	7.82	Immature
CH2	Serowe	D7	272.66	273.25	0.77	High- Volatile Bituminous: A	9.21	Mature
CH2	Serowe	D9	276.19	276.42	1.52	Medium- Volatile Bituminous	12.20	Mature
DOLERITE: 297.2-346.9 m								
CH2	Serowe	D11	357.55	357.85	1.57	Medium- Volatile Bituminous	12.38	Mature
CH8	Serowe	D2	374.29	374.67	0.4	Sub- Bituminous-C	7.54	Immature
CH8	Serowe	D5	386.81	387.41	0.62	High- Volatile Bituminous: B	8.55	Mature
CH8	Serowe	D12	391.07	391.66	0.9	High- Volatile Bituminous: A	9.77	Mature
DOLERITE: 419-491.4								

Figure 22: Maturity and proximity to dolerite intrusion in boreholes CH2 and CH8. Heat affected samples are highlighted in yellow. Dolerite intervals are denoted in blue.

5.2 Proximate Analysis

Results of the proximate analysis indicate three clusters (Figure 23) in the sample distribution. Cluster 1 is non-heat affected with %Ro ranging from 0.44% to 0.65%. Cluster 2 samples are slightly heat affected with %Ro ranging between 0.77% and 1.91%. Cluster 3 is the devolatilized or burnt coal samples with %Ro of approximately 4% and greater. These clusters correspond with the three zones distinguished earlier. Cluster 1 displays the highest moisture content range from 2.42% to 6.36%, in cluster 2 the range is from 0.76% to 3.14%, and cluster 3 ranging from 1.3 % to 3.4%. Surprisingly, moisture of the slightly heat affected samples is less than that of the devolatilized samples. According to Jiang et al. (2011) this may occur as a result of the intrusion acting as a seal to prevent moisture loss after the magmatic intrusion. This observation may hold as the devolatilized samples are within the contact metamorphism zone (2- 12 m from nearest sill).

Cluster 3 displays the lowest volatile matter content proving that with increasing heat effects from intrusion, devolatilization occurs. Thermally evolved cluster 2 shows higher

fixed carbon than cluster 1. These results are generally in agreement with those of Jiang et al. (2011) and Rimmer et al. (2009) who both state that intrusions on coal seams result in increases in fixed carbon and %Ro and decreases in volatile matter and moisture adjacent to the igneous intrusion. Cluster 3 exhibits a decrease in fixed carbon and an increase in ash and with increasing %Ro. According to Golab (2003) this is because at higher temperatures where coking begins, anisotropic vitrinite becomes isotropic and crystallises to form semi-coke, macerals decompose simultaneously, reflectance increases and reactions forming carbon dioxide, methane and other products use up part or all of the organic matter. Therefore, the fixed carbon content deteriorates whereas the ash content in these post-mature samples increases.

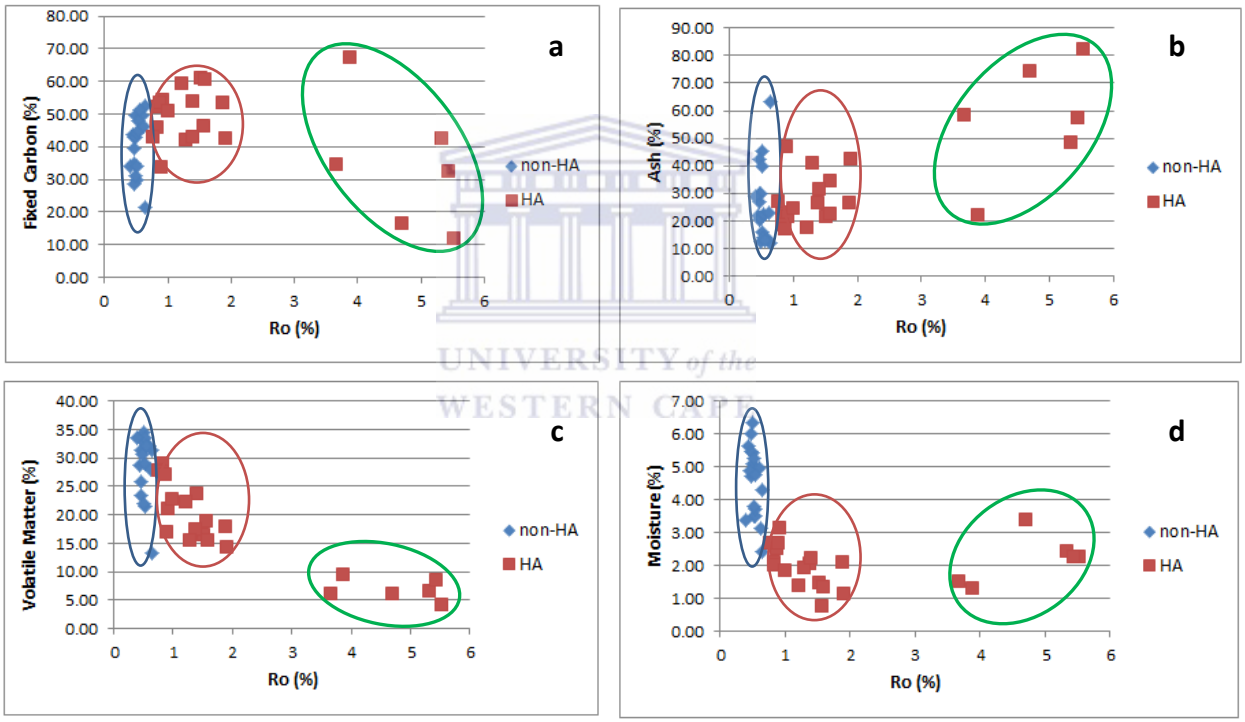

Figure 23: Correlations between %Ro and fixed carbon, moisture, volatile matter and ash contents. Cluster 1 represents non-heat affected (encircled in blue), cluster 2 represents slightly heat affected (encircled in red) and devolatilized samples (encircled in green) are represented by cluster 3. Appendix D provides proximate analysis results for boreholes CH1- CH9.

An exception in cluster 3, sample 25G from CH7 with %Ro of 3.88% (Figure 24), displays the highest fixed carbon measurement of 67.18% and 22.10% ash content, this is possibly due to the fact that it has not reached the post maturity phase of Ro> 4% and is in an early stage of semi- coking. It is also possible that following the intrusion, sample 25G underwent significant carbonate mineralization in fractures and voids and as a result, its fixed carbon

content was elevated. On the other hand, meta-anthracitic sample D3 of CH4 with %Ro of 5.53% displays fixed carbon of 11.57% and 81.96% ash content suggestive of an advanced coking stage.

Well	Sample No.	Top Depth (m)	Bottom Depth (m)	Ro (%)	LOM	Fixed Carbon (%)	Moisture (%)	Ash (%)	Volatile Matter (%)
CH4	D1	381.6	382.31	1.91	13.54	42.37	1.13	42.25	14.25
DOLERITE: 392.3-426.5 m									
CH4	D3	438.25	438.6	5.53	19.26	11.57	2.27	81.96	4.21
CH4	D7	451.19	451.77	0.84	9.52	52.22	1.99	18.33	27.46
CH4	D15	479.97	480.52	0.87	9.64	53.20	2.50	17.16	27.13
CH4	D18	488.31	488.85	1.59	12.45	60.61	1.34	22.55	15.50
DOLERITE: 505.5-507.9 m									
DOLERITE: 374.8-375.6 m									
CH7	2G	404.28	404.88	0.5	8.00	31.01	6.36	29.78	32.85
CH7	11G	432.92	433.51	0.54	8.19	47.81	4.78	13.91	33.51
CH7	16G	440.22	440.82	0.54	8.19	44.95	3.52	22.65	28.88
CH7	21G	462.81	463.09	0.55	8.23	51.33	3.72	12.91	32.05
CH7	25G	485.62	486.22	3.88	18.13	67.18	1.30	22.10	9.42
DOLERITE: 500.4-522.7 m									

Figure 24: Proximate analysis results of boreholes CH4 and CH7. Heat affected samples are highlighted in yellow. Dolerite intervals are denoted in blue.

5.3 Passey's TOC Outputs

Passey's TOCs and TOCd were determined using equations:

$$TOCs = SlogR * 10^{(0.297 - 0.1688 * LOM)} \ldots. (3)$$
$$TOCd = DlogR * 10^{(0.297 - 0.1688 * LOM)} \ldots. (4)$$

All input parameters for Passey's ΔLogR technique for boreholes CH1- CH9 are tabulated in Appendix E. In borehole CH1 (Figure 25), TOCd and TOCs estimates are generally good; the strength of their correlation with fixed carbon is shown in Figure 26. Sample 1_8G displays a higher density compared to the other samples indicating that it is less porous, which is also proven by the lowest transit time. Due to the highly compacted nature of the coal and intercalation with mudstone (high gamma ray reading), sample 1_8G resulted in the poorest estimation of TOCs and TOCd. This is most probably a consequence of the porosity logs' failure to detect low velocity and low density kerogen in the DLogR and SLogR separations of denser intervals.

Well	Sample No.	Top Depth (m)	Bottom Depth (m)	Density (g/cc)	Gamma (API-GR)	Lateral (ohm-m)	Sonic (µsec/m)	LOM	TOCd (%)	TOCs (%)	Fixed Carbon (%)	Comments
CH1	1_2G	246.12	246.59	1.45	57.63	77.98	401.83	7.72	34.65	28.83	43.49	CD: Pyrite, calcite
CH1	1_4G	268.8	269.4	1.43	66.53	146.50	410.58	7.86	35.73	31.49	42.82	CD: Pyrite, sideritic
CH1	1_5G	275.5	275.7	1.27	52.76	188.63	418.81	7.96	39.20	32.84	42.84	CD: Pyrite nodules
CH1	1_6G	277.76	278.35	1.36	63.74	191.38	423.49	7.86	38.48	34.98	39.46	CD: Pyritic
CH1	1_8G	279.9	280.11	1.94	161.49	77.26	358.12	8.00	20.12	18.11	49.62	CD-CM1: Pyrite, calcite
CH6	D2	319.78	320.37	1.55	73.73	82.88	391.12	7.86	44.97	37.77	28.41	C3
CH6	D8	329.01	329.56	1.56	88.07	82.53	384.60	8.05	44.58	36.05	44.04	C3: Sideritic
CH6	D13	340.22	340.8	1.31	22.16	141.40	420.54	8.46	55.93	48.47	49.41	C3: Sideritic
CH6	D16	356.27	356.86	1.80	217.33	27.65	344.46	8.68	30.58	19.38	21.30	CD

Figure 25: TOCd and TOCd estimates for boreholes CH1 and CH6. CD= Dull coal (<10% Bright), CM1= Carbonaceous mudstone and C3= Dull coal with frequent bright bands (10-40% Bright).

CH1 did not intercept any dolerites, all samples are immature but high resistivity responses in samples 1_4G, 1_5G and 1_6G suggest earlier biogenic gas generation. Correlation between fixed carbon and measured TOC in borehole CH6 (Figure 26) does not display very strong relationships similar to those of CH1. Nonetheless, both CH1 and CH6 yield TOCs and TOCd estimates closer to fixed carbon measurements than boreholes where sills were encountered.

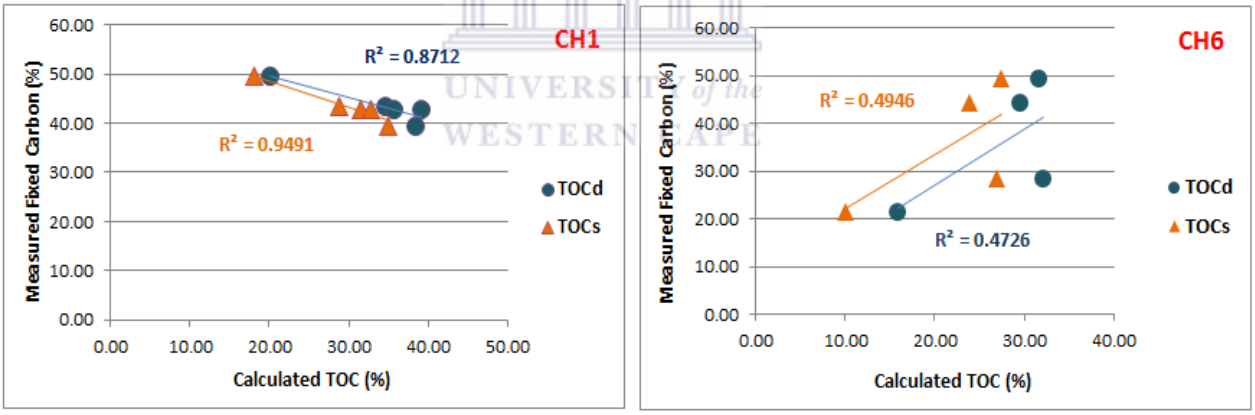

Figure 26: Correlation between calculated TOC and measured fixed carbon. CH1 shows a very strong correlation whereas CH6 shows a moderately strong correlation.

In borehole CH2 (Figure 27), only the TOCd estimate for thermally immature sample D3 is reasonable in comparison with its fixed carbon measurement. The heat affected samples D7, D9 and D11 estimations are very low compared to lab measurements as a result of a higher LOM. This can also be observed in heat affected samples of all the other boreholes. Also, D11 has been metamorphosed to a stony carbonaceous coal; this coupled with a comparatively higher LOM has immensely affected the TOC outputs.

Well	Sample No.	Top Depth (m)	Bottom Depth (m)	Density (g/cc)	Gamma (API-GR)	Lateral (ohm-m)	Sonic (usec/m)	LOM	TOCd (%)	TOCs (%)	Fixed Carbon (%)	Comments
CH2	D3	257.99	258.6	1.55	42.21	61.61	397.38	7.82	32.49	25.98	34.82	CD: Pyrite, sideritic
CH2	D7	272.66	273.25	1.61	73.20	41.96	410.64	9.21	15.27	15.65	42.78	CD-C3: Pyrite, calcite
CH2	D9	276.19	276.42	1.33	79.06	23.76	433.49	12.20	5.53	5.26	60.81	C3
DOLERITE: 297.2-346.9 m												
CH2	D11	357.55	357.85	1.89	209.62	78.16	357.75	12.38	3.73	3.30	46.02	CR

Figure 27: TOCd and TOCs estimates of CH2. Heat affected samples are highlighted in yellow. Dolerite intervals are denoted in blue. CR= Stony coal.

In borehole CH3, TOCs for D12 (Figure 28) appears to be the best estimation in this borehole and shows the significance of a lower LOM in this technique. Intercalations with coaly mudstones in D16, similar to the case of sample 1_8G of CH1; tend to give a higher density, making it difficult to recognize these zones as containing any low density organic matter in the DLogR and SLogR separations and therefore have adverse effects on the resultant TOCs/TOCd estimations.

Well	Sample No.	Top Depth (m)	Bottom Depth (m)	Density (g/cc)	Gamma (API-GR)	Lateral (ohm-m)	Sonic (usec/m)	LOM	TOCd (%)	TOCs (%)	Fixed Carbon (%)	Comments
CH3	D5	364.37	364.67	1.29	51.43	50.12	403.06	9.47	18.58	13.78	45.84	calcite, siderite
CH3	D12	374.1	374.7	1.33	40.74	74.74	411.89	8.10	32.35	26.52	29.60	Pyrite, sideritic
CH3	D13	410.25	410.48	1.67	107.37	36.00	404.16	8.64	18.23	18.20	52.44	Calcite veins
CH3	D16	418.44	419.04	1.74	265.39	36.63	392.72	9.85	10.60	10.40	54.12	Coaly mudstone
CH3	D18	421.46	422.06	1.50	155.00	45.55	422.10	11.72	6.59	6.45	53.88	Pyrite, calcite
DOLERITE: 431.7-460.7 m												

Figure 28: TOCd and TOCs estimates of CH3. Heat affected samples are highlighted in yellow. Dolerite intervals are denoted in blue. CR= Stony coal.

Other coal intersections showed little to no response in resistivity values indicating extremely low permeability, examples are seen in meta-anthracitic sample 2 of borehole CH5 and D28 of borehole CH9 (Figure 29) which have been heat altered to stony coal.

Well	Sample No.	Top Depth (m)	Bottom Depth (m)	Density (g/cc)	Gamma (API-GR)	Lateral (ohm-m)	Sonic (usec/m)	LOM	TOCd (%)	TOCs (%)	Fixed Carbon (%)	Comments
CH5	1	247.38	248.11	1.72	73.78	18.36	397.97	10.19	9.43	7.85	50.94	Coaly mudstone
DOLERITE: 268.4-281.8 m												
CH5	2	283.29	283.54	2.02	89.43	-0.31	357.92	19.25	#NUM!	#NUM!	42.50	Baked
DOLERITE: 294.3-295.1 m												
DOLERITE: 311.7-314.2 m												
CH5	5	327.09	329.78	1.58	83.23	68.18	416.62	11.76	7.00	6.19	42.83	Carbonaceous mudstone
CH5	9	335.57	336.6	1.46	86.25	79.88	423.43	11.07	10.10	8.64	59.25	Coaly mudstone
CH5	11	343.52	344.56	1.91	146.78	27.45	394.95	19.26	0.24	0.24	32.30	Carbonaceous mudstone
DOLERITE: 350.5-351.9 m												
DOLERITE: 353.6-381.8 m												
CH9	D2	406.4	407	1.68	56.33	19.73	398.63	8.05	19.70	24.19	34.21	CD: Calcite cleats
DOLERITE: 419.6-420.9 m												
CH9	D8	421.3	421.9	2.17	94.97	24.80	302.51	17.81	0.22	0.19	34.37	CR: Pyrite
CH9	D18	444.6	445.2	1.57	134.03	71.33	350.62	11.38	7.37	5.67	41.97	CM2-CR: Pyrite
DOLERITE: 455.9-498.4 m												
CH9	D28	504.8	505.4	1.97	173.00	1.40	418.45	19.00	0.05	0.25	16.38	CM2-CR: Pyrite
CH9	D31	521.2	521.8	1.44	58.14	66.32	363.02	13.44	3.61	2.77	53.46	CD: Pyrite nodules
DOLERITE: 525.9-542.7												

Figure 29: Poor resistivity responses from high LOM, burnt coal intervals in boreholes CH5 and CH9.

In their work Passey et al. (1990) state that TOCs accuracy is superior to that of TOCd and suggested that this could be due to the sensitivity of density readings to adverse hole conditions and the presence of heavy minerals such as pyrite. In this study, TOCs does not display any superiority to TOCd, in fact its accuracy is poorer to that of TOCd in some cases. Density of the samples controls both density and sonic log readings. Most sampled intervals are pyritic and don't necessarily exhibit higher densities due to its presence. Passey's method is effective in identifying coal as organic rich zones and potential source rocks. However, accuracy in its TOCs/TOCd predictions depends on selected baseline readings, density and more so, on the LOM of the coal. LOM has proved to be a significant and sensitive parameter in this method. Figure 30 shows that with increasing LOM, TOC estimates deteriorate, resulting in poor correlations with fixed carbon measurements.

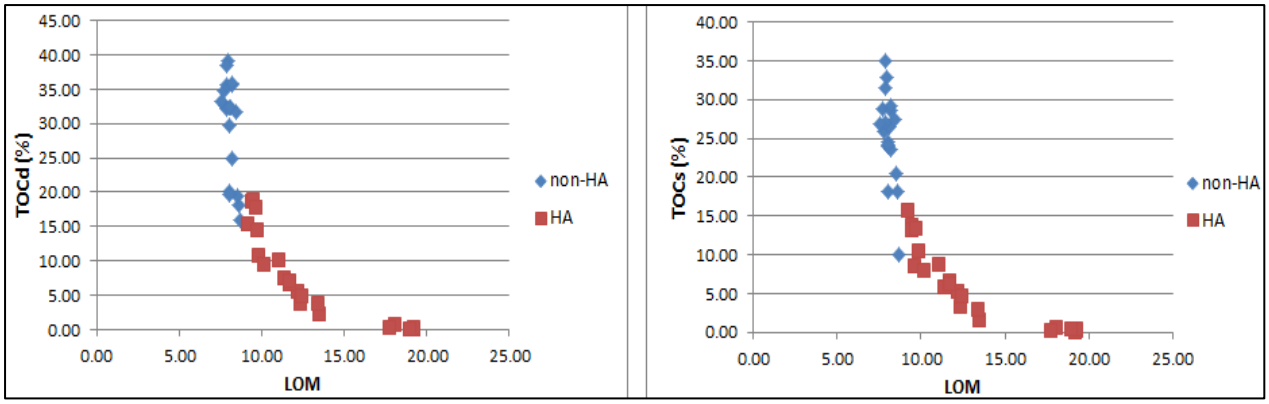

Figure 30: The relationship between LOM and calculated TOC in heat affected (HA) and non-heat affected (non-HA) samples.

Coal that has undergone normal burial metamorphism compositionally varies from the rapidly heat altered coal. %Ro increased from 0.44% in non- heat affected coal to 5.53% in the contact metamorphism zone. Adjacent to the intrusion, there is a decrease in volatile matter, moisture decreases then slightly increases as sealed by the intrusion; fixed carbon increases then decreases as vitrinite decomposes and semi-coke begins to form. Ash content increases adjacent to the intrusion. According to Rimmer et al. (2009) these geochemical changes reflect increasing rank approaching the intrusion.

Due to a high LOM and associated geochemical changes TOCd and TOCs quantification is poor in heat affected coal as shown by the major underestimations in Figure 31. Inaccuracy in all heat affected samples is very high, ranging from approximately 20% up to 65%. It is also clear from Figure 31 that TOCd and TOCs quantification is more superior in non-heat affected coal as accuracy and minimal inaccuracy are attained in some samples.

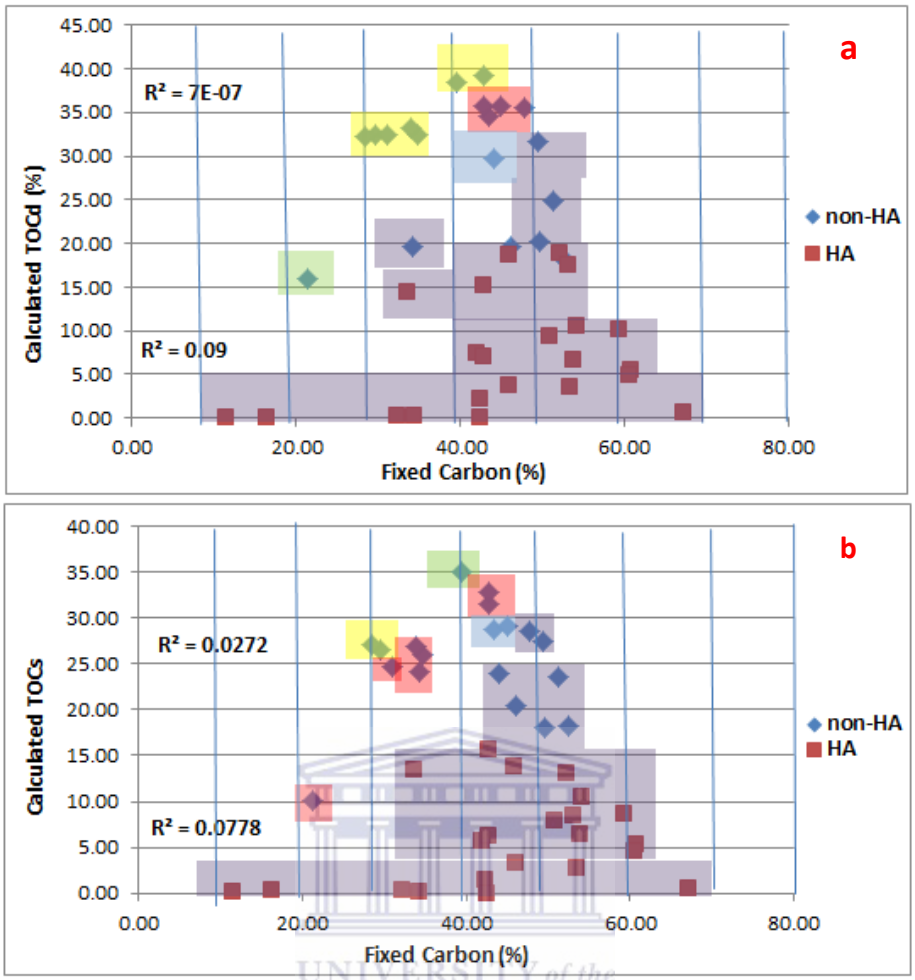

Figure 31: Poor correlations between fixed carbon and calculated TOCd (a) and TOCs (b). Colour coding: The yellow blocks indicate where there is a direct 1:1 correlation between fixed carbon and calculated TOC. Green is within within 0-5% inaccuracy, Red is within 5-10% inaccuracy, blue is within 10-15% inaccuracy and purple represents >15% inaccuracy.

5.4 Shortcomings of Passey's ΔLogR method

Selection of the baseline interval is subjective as numerous baselines occur across the borehole various depths. Although some baselines in a borehole display similar measurements, deeper baselines are quite different from shallower ones. For instance, baselines selected at 250 m display different values to those selected at 500 m as older shales generally display higher resistivities than younger ones. Also, compaction with burial will result in higher densities and faster transit time in the older shale sequence. These input parameters have an impact on calculated TOCs/TOCd predictions. Passey's method does not provide any criteria for selection of a baseline interval. In their work, Sun et al. (2013) found that ΔLogR method does not work very well and this may be due to the failure of an artificially selected baseline. In this study, a baseline was selected per well, and for

consistency in %TOC results, these baselines were selected at depths of between 300 m and 400 m, mostly lying within mudstones of the Tlhabala Formation.

Rezaee (2015) emphasizes that although this method is used extensively for determining %TOC in shale formation evaluations; there are some uncertainties to it. For instance, it requires similar conductive minerals such as pyrite in both the baseline and organic-rich intervals. Rezaee (2015) also states that vertical heterogeneity of shale sequences could result in high uncertainties for calculated %TOC. In this study, geological logs indicate that pyrite does occur in both organic rich coals and clayey baseline intervals as scattered patches and nodules. The baseline intervals selected in this study consist of very homogeneous and massive mudstone with minor siltstone. Therefore uncertainty due to factors stipulated by Rezaee (2015) is limited.

Coals in the basin are generally sideritic and comprise calcite infilled cleats or microveins (Appendix E). The proximate analyses procedure did not incorporate removal of any carbonate concentration which may have contributed to the fixed carbon content as fixed carbon does not differentiate between inorganic or organic carbon. Commonly, the amount of carbonate concentration is determined by acid digestion where the carbon dioxide generated is measured and then subtracted from the total carbon dioxide to obtain the organic fraction (Charsky and Herron, 2013). Although coals generally have high fixed carbon contents, it is possible that minor carbonate quantities may have contributed to the total fixed carbon amount and may be the cause of inaccuracy in some calculated %TOC using the ΔLogR technique as it only detects organic carbon.

Rezaee (2015) disagrees with the theory by Passey et al. (1990), which states that an increase in the amount of hydrocarbons generated at a higher LOM can be correlated to the %TOC present in the source rock. According to Rezaee (2015), this assumption is flawed because the quantity of hydrocarbons within pores depends on both the LOM and initially deposited TOC (iTOC), and not on the quantity of the %TOC present in the source rock. Therefore as a result, the ΔLogR separation between the resistivity and porosity logs may be correlated to (iTOC) and not present %TOC.

5.5 Fixed Carbon Correlations with Log Suite

Fixed carbon contents of non- heat affected samples display no correlations with the log suite at all (Figure 32). Interestingly, samples from immature boreholes CH1 and CH6 display the highest resistivities of between 141.4 and 191.38 ohm-m; most probably linked to their generation of biogenic gas. Cokar et al. (2010) state that biogenic gas is a result of shallow subsurface metabolism of organic matter by micro-organisms. Its generation depends on geological, geochemical, biochemical and hydrological properties of the formation.

One would expect thermally immature coals to show very low resistivity readings, because biogenic gas generation is not temperature dependant, these samples have generated and stored some biogenic gas during diagenesis. Therefore, it is clear that biogenic and thermogenic regimes contributed to gas generation in the basin. And since most of the thermogenic gas was not adsorbed on to the coals as discussed in section 3.1, it seems most of the gas present in the coals is of biogenic origin.

Heat affected samples display a poor correlation (R^2= 0.319) with resistivity (Figure 32-a) suggesting the escape of some thermogenic gas or possibly a result of the hindrance by increases in density which have adverse effects on porosity and permeability, leading to very poor resistivity responses especially in samples with %Ro> 3% as discussed in section 5.3. This is collaborated by a similar existing relationship, although poor (R^2= 0.338), displayed by decreasing fixed carbon with increasing density (Figure 32-c) in heat affected samples.

There appears to be neither relationship at all in neither gamma ray nor transit time in heat affected nor non-heat affected coals due to the fact that coals in the region are intercalated with mudstone and silt. Some source rock coals are actually carbonaceous mudstones, the lithology in the area is generally clay enriched. This results in high gamma ray and faster transit time in some intervals. Overall, very poor relationships exist (R^2 of 0.003 to 0.338) between fixed carbon and any log indicating that no single curve can be used to predict fixed carbon or TOC contents in a given borehole.

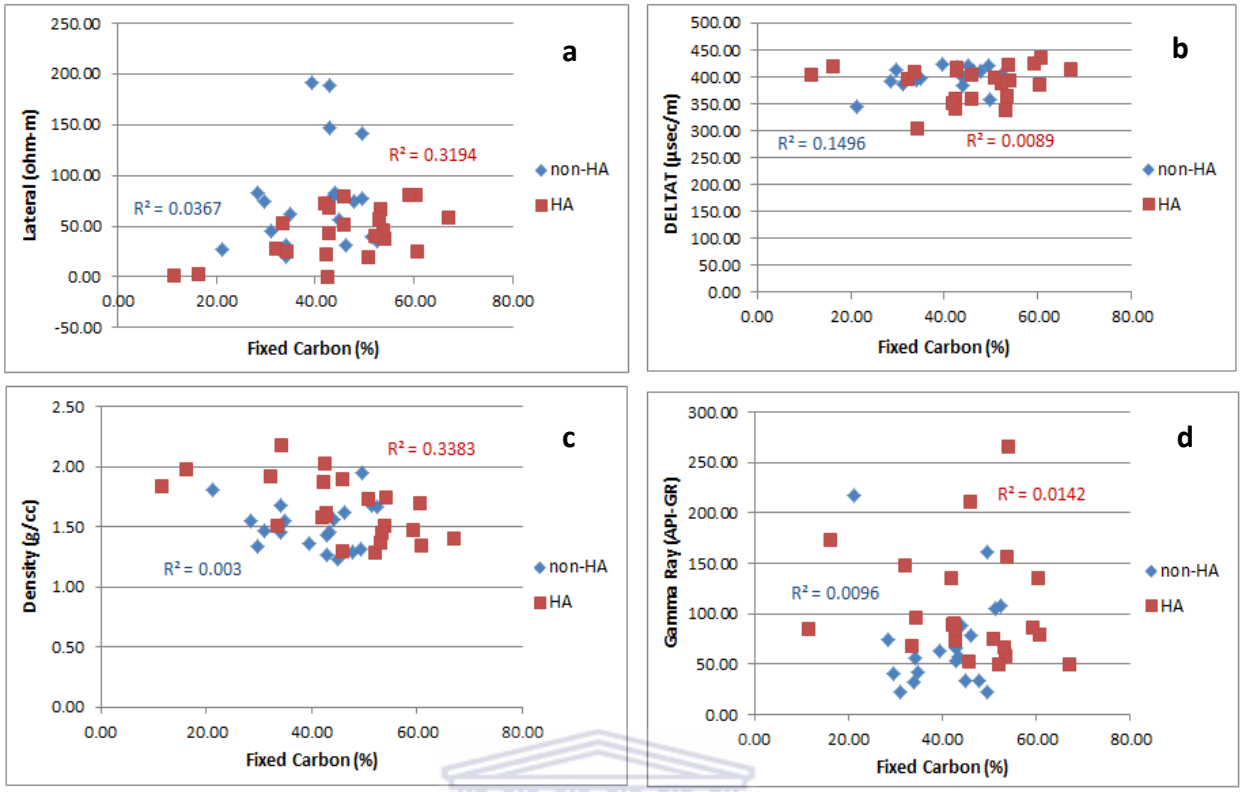

Figure 32: Fixed Carbon correlations with (a) resistivity, (b) sonic (c) density and (d) gamma ray curves.

5.6 Application of Passey's ΔLogR: Generating TOC curves in IP

Vitrinite reflectance measurements were conducted on only 41 cored intervals. In the remaining intervals LOM can be estimated, however this can only be done in boreholes CH1 and CH6 where maturity is believed to have been due to geothermal gradients and burial only. LOM ranges are 7.72 to 8 and 7.86 to 8.68 for CH1 and CH6, respectively. Therefore, in both boreholes an average LOM value within a reasonable range can be used to generate %TOC estimation curves for the entire borehole. In dolerite heat influenced boreholes, using an average LOM would lead to very erroneous TOC estimates as the LOM ranges are too wide and are not depth dependant. For example, CH4 and CH7 display LOM ranges of 9.52 to 19.26 and 8 to 18.13, respectively.

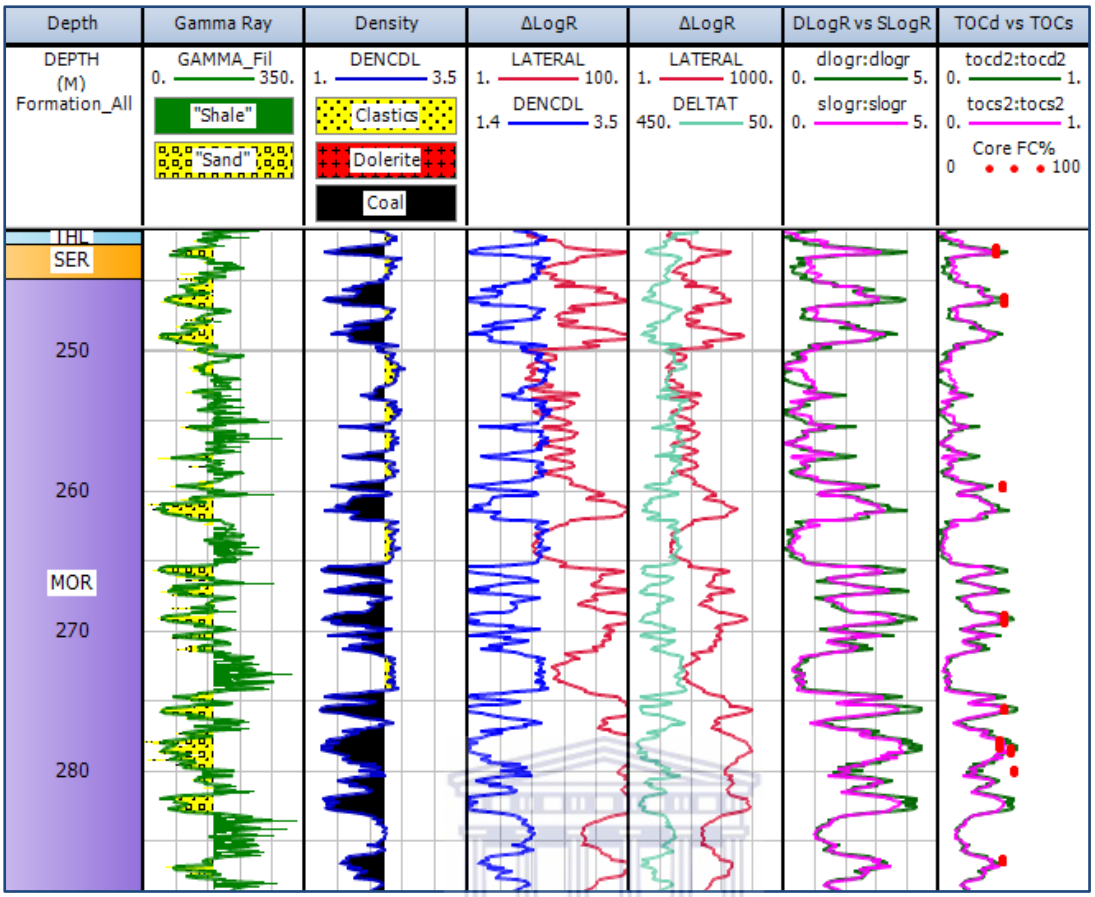

Figure 33: TOCd and TOCs curves displayed with fixed carbon (FC %) core measurements in borehole CH1. Tracks 4 and 5 indicate the ΔLogR separation in log overlays.

Figure 33 shows ΔLogR separations in both lateral-density and lateral-sonic combinations. DLogR and SLogR curves (Figure 33, Track 6) were calculated from the separations and converted to quantitative TOCs and TOCd curves (Figure 33, Track 7) using an average LOM of 7.8. Correlation with fixed carbon indicates that generally, there is a very strong relationship between calculated and measured variables as shown in Figure 34.

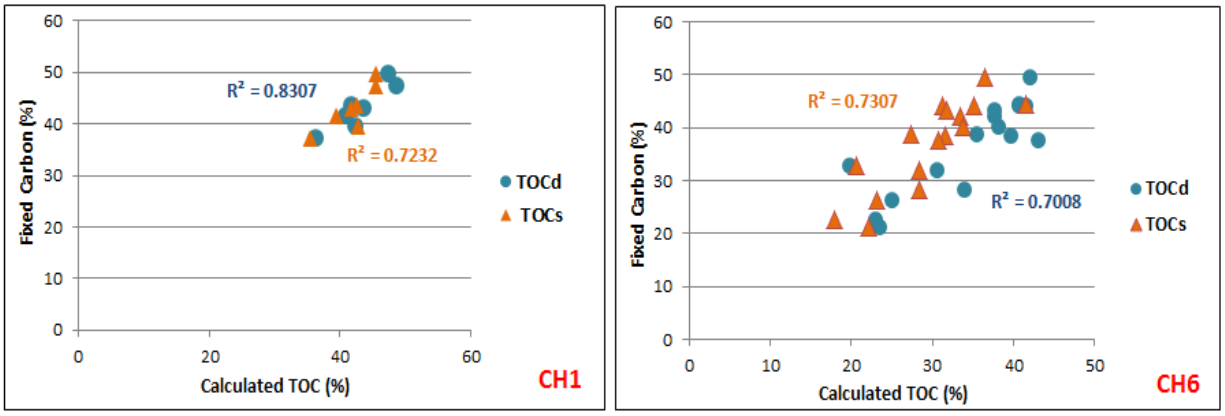

Figure 34: Correlation between calculated TOC and measured fixed carbon in boreholes CH1 and CH6.

In CH6 (Figure 35), an average LOM value from sampled intervals of 8.26 was used in the TOCs and TOCd curves calculation. Figure 34 indicates that TOCd estimations are stronger than TOCs in both boreholes contradicting the theory by Passey et al. (1990). Essentially in both boreholes, Passey's TOC curves mostly align well with core measurements and although not accurate, the curves indicate that the method can be applied to coal that has not been thermally altered by igneous sills and dykes.

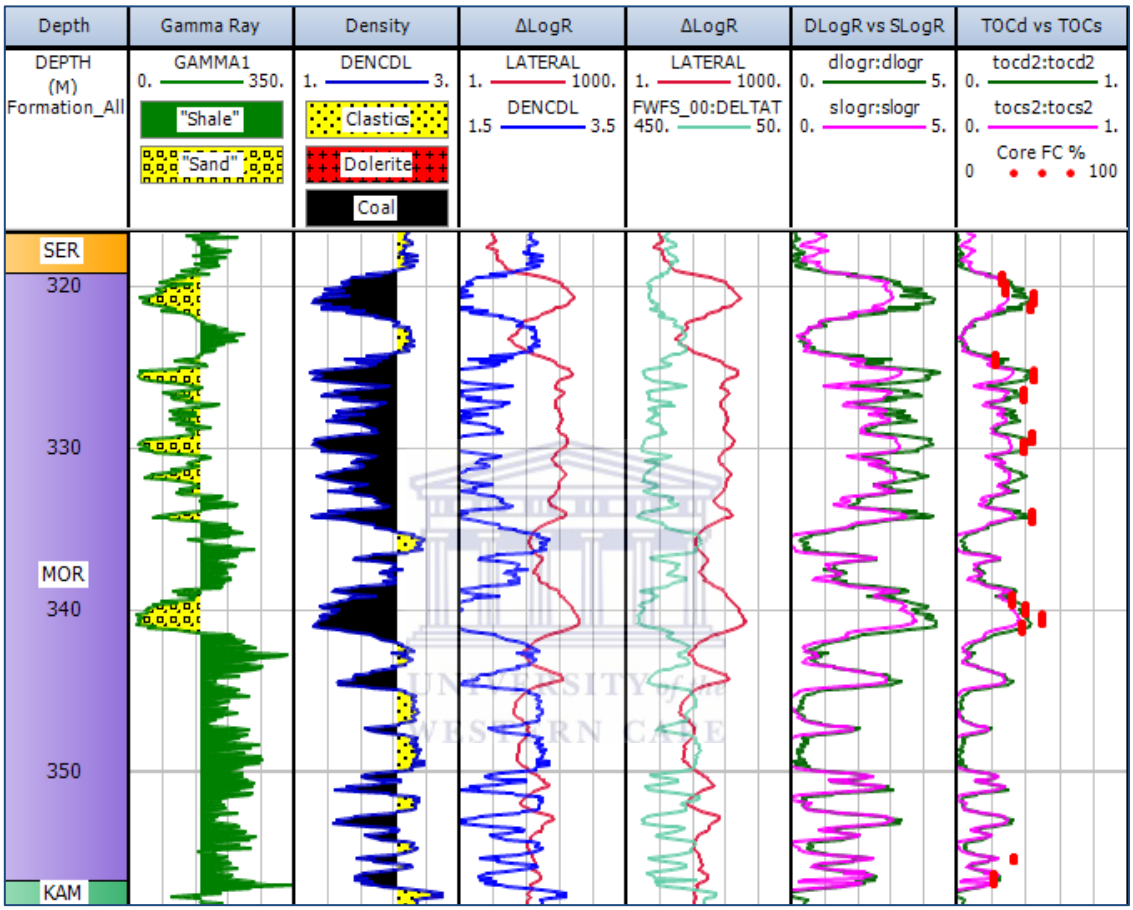

Figure 35: TOCd and TOCs curves calibrated to Fixed Carbon (FC %) core measurements in borehole CH6.

6. Conclusions and Recommendations

Passey's ΔLogR has effectively identified coal intervals of the Central Kalahari Karoo Basin as organic rich. Comparison with fixed carbon lab measurements indicates that Passey's method can be applied in quantifying %TOC in non- heat altered coal provided there are minimal intercalations with mudstone or siltstone which tend to increase the density of the coal interval. The method however, yields very poor TOC estimations and does not apply in coal altered by heat effects from igneous intrusion as a consequence of:

- High LOM. High temperatures associated with these intrusions have elevated the LOM of the coal. The higher the LOM, the lower the accuracy in TOC predictions.
- Accompanying compositional changes. At higher temperatures where coking begins, anisotropic vitrinite becomes isotropic and crystallises to form semi-coke (devolatilized coal) (Golab, 2003). With increasing %Ro, macerals decompose simultaneously thereby increasing ash content and decreasing fixed carbon towards the intrusion. Volatile matter contents are the lowest in the contact metamorphism zone. Moisture decreases in the thermal evolution zone then slightly increases in the contact metamorphism zone as sealed by the intrusion itself.
- Increased coal rank and subsequent increase in density resulting in minimal or no resistivity responses which are required in Passey's TOC calculations.

LOM has proved to be a very crucial input parameter as it controls TOC outputs immensely hence it should be estimated correctly. Generated TOC curves of boreholes CH1 and CH6 that did not intercept dolerites show a very strong correlation with measured fixed carbon. Therefore, this shows that the technique can achieve accuracy in its predictions. Although it is typical for coals to have high fixed carbon contents, there is an abundance of siderite and calcite mostly infilling cleats as documented in geological logs. Since no procedure for the correction of any carbonates was done, fixed carbon includes both organic and inorganic carbon. The presence of these carbonates could possibly have a minor influence on fixed carbon content which the ΔLogR separation would not detect as it only responds to organic carbon. So there is uncertainty regarding the presence of inorganic carbon. With regards to methane gas generation in the basin, correlations between fixed carbon and the log suite have revealed the presence of some biogenic gas in thermally immature samples. Therefore

both biogenic and thermogenic processes seem to have contributed to methane generation in the basin.

Recommendations

- For future work, more research needs to be conducted on Passey's ΔLogR technique so that it can also be applied to coal heat altered by magmatic intrusions as coal is increasingly becoming prospective for CBM reserves.
- Alternative methods such as Carbolog and the Optimal Superposition technique should be looked into for quantification of %TOC in coal thermally altered by igneous intrusions. Both methods do not require selection of a baseline interval or LOM in their calculations. Although these methods are currently poorly understood, with more research they could potentially be useful in coal source rock analysis.
- Acid digestion of present carbonates in coal should always be performed prior to proximate analysis to remove any possible effects of carbonate decomposition on analysis results. This will also remove the inorganic carbon and reduce uncertainties if attempting to calculate %TOC, as in this study.
- In order to supplement proximate analysis results, if possible, Rock-Eval pyrolysis should be conducted on decarbonated coal samples as it will provide direct %TOC measurements.

7. Bibliography

Advanced Resources International (ARI), Inc. (2003). Results of the Central Kalahari Karoo Basin coalbed methane feasibility study. Open file archives, Geological Survey Department, Botswana.

Andersen, N. and Potgieter, J. (2012). An evaluation of the methane potential of the central Kalahari area of Botswana from a Geological Prespective. For Kubu Energy Resources.

Bennett, J.D. (1989). Review of Lower Karoo coal basins and coal resource development in parts of central and southern Africa with particular reference to northern Malawi. *Technical Report WC/89/21 British Geological Survey.*

Berch, H.C. (2013*). Predicting Potential Unconventional Production in the Tuscaloosa Marine Shale Play Using Thermal Modeling and Log Overlay Analysis*. United States of America: Louisiana State University. (PhD Thesis).

Bordy, E.M., Segwabe, T. and Makuke, B. (2010). Sedimentology of the Upper Triassic-Lower Jurassic (?) Mosolotsane Formation (Karoo Supergroup), Kalahari Karoo Basin, Botswana. *Journal of African Earth Sciences*. 58: 127- 140.

Carney, J. N., Aldis, D. T. and Lock, N.P. (1994). *The Geology of Botswana*. Bulletin 37, Geological Survey Department, Botswana.

Catuneanu, O., Wopfner, H., Eriksson, P.G., Cairncross, B., Rubidge, B.S., Smith, R.M.H. and Hancox, P.J. (2005). The Karoo Basins of south-central Africa. *Journal of African Earth Sciences* 43: 211- 253.

Charsky, A. and Herron, S. (2013). Accurate, Direct Total Organic Carbon (TOC) Log from a New Advanced Geochemical Spectroscopy Tool: Comparison with Conventional Approaches for TOC Estimation. In *AAPG Annual Convention and Exhibition.* Search and Discovery Article: 41162. Pittsburg, Pennsylvania, May 19-22, 2013. AAPG.

Cokar, M., Kallos, M. S., Huang, H., Larter, S.R. and Gates, I.D. (2010). Biogenic Gas Generation From Shallow Organic-Matter-Rich Shales. In *Canadian Unconventional Resources & International Petroleum Conference.* CSUG/SPE 135323. Alberta, Canada, 19-21 October 2010. Society of Petroleum Engineers.

Crain, E.R. (2013). Your first and only eText Reference Manual and Home Study Course in Petrophysics and Well Log Analysis. Total Organic Carbon (TOC) Basics. [Online] Available from: http://www.spec2000.net [Accessed: 11 June 2015].

Faiz, M., Crozier, E. and Lee-King, A. (2013). *Influence of Coal Type, Rank and Thermal History on Gas Contents in the Kubu PLs, Botswana*. Kubu Energy Report. Unpublished.

Faiz, M., Murphy, A., Hendry, P. and Midgley, D. (2012). Geochemical and Microbiological Review of Coal Seam Gas – New Facts and Old Controversies. in *Eastern Australian Basin Symposium*. Commonwealth Scientific and Industrial Research Organisation. Brisbane, 13 September 2012.

Flores, R. M., Rice C. A., Stricker, G.D., Warden, A. and Ellis, M.S. (2008). Methanogenic pathways of coal-bed gas in the Powder River Basin, United States: The geologic factor. *International Journal of Coal Geology*. 76: 52- 75.

Golab, A. (2003). *The impact of igneous intrusions on coal, cleat carbonate and groundwater composition.* University of Wollongong. (PhD Thesis).

Haddon, I.G. (2005). *The sub-Kalahari geology and tectonic evolution of the Kalahari Basin, Southern Africa*. Johannesburg: University of the Witwatersrand. (PhD Thesis).

Hood, A., Gutjahr, C. M., and Heacock, R. L. (1975). Organic Metamorphism and the Generation of Petroleum. *The American Association of Petroleum Geologists Bulletin.* 59 (6): 986- 995.

Jarvie, D. M. (1991). Total Organic Carbon (TOC) Analysis. In R. K. Merrill (Ed.), *Treatise of Petroleum Geology: Handbook of Petroleum Geology*: Source and Migration Processes and Evaluation. Tulsa: American Association of Petroleum Geologists.

Jiang, J., Cheng, Y., Wang, L., Li, W. and Wang, L. (2011). Petrographic and geochemical effects of sill intrusions on coal and their implications for gas outbursts in the Wolonghu Mine, Huaibei Coalfield, China. *International Journal of Coal Geology.* 88: 55- 66.

Jourdan, F., Féraud, G., Bertrand, H., Watkey, M.K., Kapunzu, A.B. and Le Gall, B. (2006). Basement control on dyke distribution in Large Igneous Provinces: Case study of the Karoo triple junction. *Earth and Planetary Science Letters.* 241: 307- 322.

Le Gall, B., Tshoso, G., Jourdan, F., Féraud, G., Bertrand, H., Tiercelin, J.J., Kampunzu, A.B., Modisi, M.P., Dyment, J. and Maia, M. (2002). $^{40}Ar/^{39}Ar$ geochronology and structural data from the giant Okavango and related mafic dyke swarms, Karoo igneous province, northern Botswana. *Earth and Planetary Science Letters.* 202: 595- 606.

Modie, B.N. (2008). *The Palaeozoic Palynostratigraphy of the Karoo Supergroup and palynofacies insight into palaeoenvironmental interpretations, Kalahari Karoo Basin, Botswana.* (PhD Thesis). Unpublished.

Ogala, J.E. (2011). Hydrocarbon Potential of the Upper Cretaceous Coal and Shale Units in the Anambra Basin, South Eastern Nigeria. *Petroleum & Coal*. 53 (1): 35- 44.

Passey, Q., Creaney, S., Kulla, J., Moretti F. and Stroud, J. (1990). A pratical model for organic richness from porosity and resistivity logs. *The American Association of Petroleum Geologists Bulletin.* 74(12): 1777- 1794.

Rainbow Gas & Coal Exploration (PTY) Ltd. (2012). Early Final Relinquishment Report for Prospecting Licenses 36- 47/2007 and 90/2007. Rainbow Gas & Coal Exploration (PTY) Ltd, Botswana.

Rao, P.L .,Rasheed, M. A., Hasan, S.Z. , Rao, P.H. and Harinarayana,T. (2014). Role of Geochemistry in Coalbed Methane - A Review. *Geosciences*. 4(2): 29- 32.

Rezaee, R. (2015). *Fundamentals of Gas Shale Reservoirs*. Hoboken, New Jersey: John Wiley & Sons.

Rice, D.D. (1993). Composition and origins of coalbed gas, in: Law, B.E., Rice, D.D. _Eds.., Hydrocarbons from Coal. *AAPG Studies in Geology*. a38: 159- 184.

Rimmer, S.M., Yoksoulian, L.E. and Hower, J.C. (2009). Anatomy of an intruded coal, I: effect of contact metamorphism on whole-coal geochemistry, Springfield (No. 5) (Pennsylvanian) coal, Illinois Basin. *International Journal of Coal Geology*. 79: 74- 82.

Roon, J. and Parker, I. (2014). Stratigraphic re-interpretations of Kubu Energy Resources Botswana coreholes 1 to 9. Unpublished report.

Segwabe, T. (2008).*The Geological Framework and Depositional Environments of the Coal-Bearing Karoo Strata in the Central Kalahari Karoo Basin, Botswana*. Rhodes University. (MSc Thesis).

Shiri, M., Ranjbar-Karami, R., Moussavi-Harami, R. and Rezaee, M. (2013). Evaluation of organic carbon content and source rock maturity using petrophysical logs and geochemical data: Case study of Horn Valley Siltstone source rock, Amadeus Basin, Central Australia. *Journal of Zankoy Sulaimani- Part A.* 15 (3): 145- 158.

Smith, R.A. (1984). The Lithostratigraphy of the Karoo Supergroup in Botswana: A Report on the Geophysical and Geological Results of Follow-up Drilling to the Aeromagnetic Survey of Botswana. Republic of Botswana, *Geological Survey Department, Bulletin 26*. Lobatse, Botswana.

Standards Association of Australia, 2000a. Australian Standards AS1038.3: Proximate Analysis of higher rank coal. Standards Association of Australia, Sydney.

Standards Association of Australia, 2000b. Australian Standards AS2456.3: Microscopical determination of the reflectance of coal macerals. Standards Association of Australia, Sydney.

Sun, S., Sun, Y., Sun, C., Liu, Z. and Dong, N. (2013). Methods of calculating total organic carbon from borehole logs and its application on rock's properties analysis. *Search and Discovery: 41372*. Beijing, China.

Underground Coal. (2011). Outburst: Rank of coal seam. [Online] Available from: http://www.undergroundcoal.com.au/outburst/rank.aspx [Accessed: 15 August 2015].

Visser, N. J. (1997). Deglaciation sequences in the Permo-Carboniferous Karoo and Kalahari basins of southern Africa: a tool in the analysis of cyclic glaciomarine basin fills. *Sedimentology*. 44: 507- 521.

APPENDIX A: (i) Resistivity and (ii) Transit time histogram distributions for all boreholes.

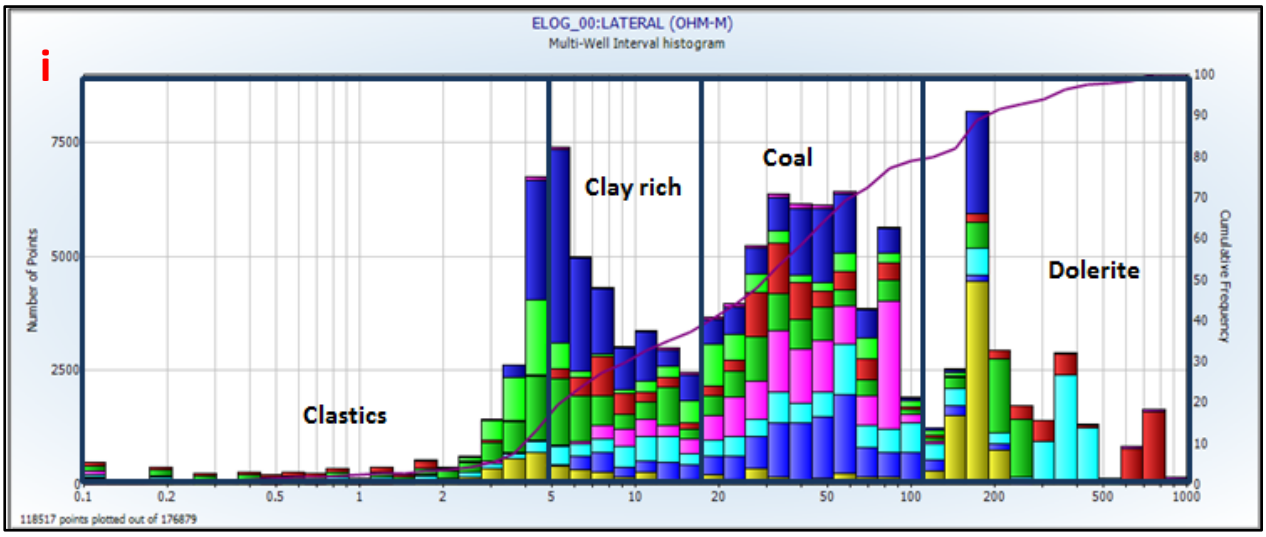

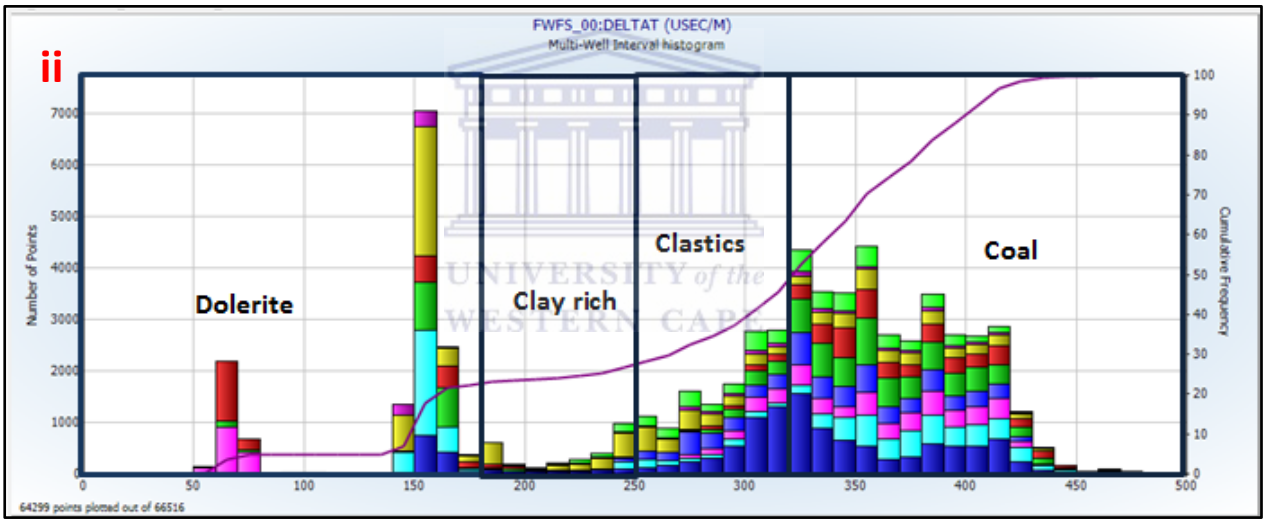

APPENDIX B: RESDbase, DENSbase and DTCbase values obtained in baseline intervals of each borehole.

Well	Sample No.	Top Depth (m)	Bottom Depth (m)	RESDbase	DENSBase	DTCbase
CH1	1_2G	246.12	246.59	10.00	2.50	300.00
CH1	1_4G	268.8	269.4	10.00	2.50	300.00
CH1	1_5G	275.5	275.7	10.00	2.50	300.00
CH1	1_6G	277.76	278.35	10.00	2.50	300.00
CH1	1_8G	279.9	280.11	10.00	2.50	300.00
CH2	D3	257.99	258.6	10.00	2.60	300.00
CH2	D7	272.66	273.25	10.00	2.60	300.00
CH2	D9	276.19	276.42	10.00	2.60	300.00
CH2	D11	357.55	357.85	10.00	2.60	300.00
CH3	D5	364.37	364.67	10.00	2.50	300.00
CH3	D12	374.1	374.7	10.00	2.50	300.00
CH3	D13	410.25	410.48	10.00	2.50	300.00
CH3	D16	418.44	419.04	10.00	2.50	300.00
CH3	D18	421.46	422.06	10.00	2.50	300.00
CH4	D1	381.6	382.31	12.00	2.60	280.00
CH4	D3	438.25	438.6	12.00	2.60	280.00
CH4	D7	451.19	451.77	12.00	2.60	280.00
CH4	D15	479.97	480.52	12.00	2.60	280.00
CH4	D18	488.31	488.85	12.00	2.60	280.00
CH5	1	247.38	248.11	14.00	2.67	300.00
CH5	2	283.29	283.54	14.00	2.67	300.00
CH5	5	327.09	329.78	14.00	2.67	300.00
CH5	9	335.57	336.6	14.00	2.67	300.00
CH5	11	343.52	344.56	14.00	2.67	300.00
CH6	D2	319.78	320.37	7.00	2.50	300.00
CH6	D8	329.01	329.56	7.00	2.50	300.00
CH6	D13	340.22	340.8	7.00	2.50	300.00
CH6	D16	356.27	356.86	7.00	2.50	300.00
CH7	2G	404.28	404.88	10.00	2.67	280.00
CH7	11G	432.92	433.51	10.00	2.67	280.00
CH7	16G	440.22	440.82	10.00	2.67	280.00
CH7	21G	462.81	463.09	10.00	2.67	280.00
CH7	25G	485.62	486.22	10.00	2.67	280.00
CH8	D2	374.29	374.67	7.00	2.50	300.00
CH8	D5	386.81	387.41	7.00	2.50	300.00
CH8	D12	391.07	391.66	7.00	2.50	300.00
CH9	D2	406.4	407	12.00	2.50	270.00
CH9	D8	421.3	421.9	12.00	2.50	270.00
CH9	D18	444.6	445.2	12.00	2.50	270.00
CH9	D28	504.8	505.4	12.00	2.50	270.00
CH9	D31	521.2	521.8	12.00	2.50	270.00

APPENDIX C: %Ro, Coal Rank, calculated LOM and Maturity Phases for sampled intervals in boreholes CH1- CH9.

Well	Formation	Sample No.	Top Depth (m)	Bottom Depth (m)	Ro (%)	Coal Rank	LOM	Maturity Phase
CH1	Serowe	1_2G	246.12	246.59	0.44	Sub- Bituminous- B	7.72	Immature
CH1	Serowe	1_4G	268.80	269.40	0.47	Sub- Bituminous- B	7.86	Immature
CH1	Serowe	1_5G	275.50	275.70	0.49	Sub- Bituminous- A	7.96	Immature
CH1	Serowe	1_6G	277.76	278.35	0.47	Sub- Bituminous- B	7.86	Immature
CH1	Serowe	1_8G	279.90	280.11	0.5	High- Volatile Bituminous: C	8.00	Immature
CH2	Serowe	D3	257.99	258.60	0.46	Sub- Bituminous- B	7.82	Immature
CH2	Serowe	D7	272.66	273.25	0.77	High- Volatile Bituminous: A	9.21	Mature
CH2	Serowe	D9	276.19	276.42	1.52	Medium- Volatile Bituminous	12.20	Mature
DOLERITE: 297.2-346.9 m								
CH2	Serowe	D11	357.55	357.85	1.57	Medium- Volatile Bituminous	12.38	Mature
CH3	Serowe	D5	364.37	364.67	0.83	High- Volatile Bituminous: A	9.47	Mature
CH3	Serowe	D12	374.10	374.70	0.52	High- Volatile Bituminous: B	8.10	Immature
CH3	Serowe	D13	410.25	410.48	0.64	High- Volatile Bituminous: B	8.64	Mature
CH3	Serowe	D16	418.44	419.04	0.92	High- Volatile Bituminous: A	9.85	Mature
CH3	Serowe	D18	421.46	422.06	1.39	Medium- Volatile Bituminous	11.72	Mature
DOLERITE: 431.7-460.7 m								
CH4	Serowe	D1	381.60	382.31	1.91	Low- Volatile Bituminous	13.54	Mature
DOLERITE: 392.3-426.5 m								
CH4	Morupule	D3	438.25	438.60	5.53	Meta- Anthracite	19.26	Post-mature
CH4	Morupule	D7	451.19	451.77	0.84	High- Volatile Bituminous: A	9.52	Mature
CH4	Morupule	D15	479.97	480.52	0.87	High- Volatile Bituminous: A	9.64	Mature
CH4	Morupule	D18	488.31	488.85	1.59	Medium- Volatile Bituminous	12.45	Mature
DOLERITE: 505.5-507.9 m								
CH5	Serowe	1	247.38	248.11	1.00	High- Volatile Bituminous: A	10.19	Mature
DOLERITE: 268.4-281.8 m								
CH5	Serowe	2	283.29	283.54	5.33	Meta- Anthracite	19.25	Post-mature
DOLERITE: 294.3-295.1 m								
DOLERITE: 311.7-314.2 m								
CH5	Serowe	5	327.09	329.78	1.4	Medium- Volatile Bituminous	11.76	Mature
CH5	Serowe	9	335.57	336.60	1.22	Medium- Volatile Bituminous	11.07	Mature
CH5	Serowe	11	343.52	344.56	5.44	Meta- Anthracite	19.26	Post-mature
DOLERITE: 350.5-351.9 m								
DOLERITE: 353.6-381.8 m								
CH6	Serowe	D2	319.78	320.37	0.47	Sub-Bituminous- B	7.86	Immature
CH6	Serowe	D8	329.01	329.56	0.51	High- Volatile Bituminous: C	8.05	Immature
CH6	Serowe	D13	340.22	340.8	0.6	High- Volatile Bituminous: B	8.46	Mature
CH6	Morupule	D16	356.27	356.86	0.65	High- Volatile Bituminous: B	8.68	Mature
DOLERITE: 374.8-375.6 m								
CH7	Serowe	2G	404.28	404.88	0.5	High- Volatile Bituminous: C	8.00	Immature
CH7	Serowe	11G	432.92	433.51	0.54	High- Volatile Bituminous: B	8.19	Immature
CH7	Serowe	16G	440.22	440.82	0.54	High- Volatile Bituminous: B	8.19	Immature
CH7	Serowe	21G	462.81	463.09	0.55	High- Volatile Bituminous: B	8.23	Immature
CH7	Serowe	25G	485.62	486.22	3.88	Anthracite	18.13	Mature
DOLERITE: 500.4-522.7 m								
CH8	Serowe	D2	374.29	374.67	0.4	Sub- Bituminous-C	7.54	Immature
CH8	Serowe	D5	386.81	387.41	0.62	High- Volatile Bituminous: B	8.55	Mature
CH8	Serowe	D12	391.07	391.66	0.9	High- Volatile Bituminous: A	9.77	Mature
DOLERITE: 419-491.4								
CH9	Serowe	D2	406.40	407.00	0.51	High- Volatile Bituminous: C	8.05	Immature
DOLERITE: 419.6-420.9 m								
CH9	Serowe	D8	421.30	421.90	3.67	Anthracite	17.81	Mature
CH9	Serowe	D18	444.60	445.20	1.30	Medium- Volatile Bituminous	11.38	Mature
DOLERITE: 455.9-498.4 m								
CH9	Morupule	D28	504.80	505.40	4.71	Anthracite	19.00	Post-mature
CH9	Morupule	D31	521.20	521.80	1.88	Low- Volatile Bituminous	13.44	Mature
DOLERITE: 525.9-542.7								

APPENDIX D: Proximate Analysis results for sampled intervals.

Well	Sample No.	Top Depth (m)	Bottom Depth (m)	Fixed Carbon (%)	Moisture (%)	Ash (%)	Volatile Matter (%)
CH1	1_2G	246.12	246.59	43.49	5.65	22.11	28.74
CH1	1_4G	268.8	269.4	42.82	5.45	20.23	31.50
CH1	1_5G	275.5	275.7	42.84	5.43	21.04	30.70
CH1	1_6G	277.76	278.35	39.46	4.71	29.99	25.84
CH1	1_8G	279.9	280.11	49.62	5.08	12.37	32.94
CH2	D3	257.99	258.6	34.82	4.88	26.79	33.52
CH2	D7	272.66	273.25	42.78	2.69	26.84	27.69
CH2	D9	276.19	276.42	60.81	1.45	21.45	16.30
CH2	D11	357.55	357.85	46.02	0.76	34.45	18.77
CH3	D5	364.37	364.67	45.84	2.10	22.98	29.07
CH3	D12	374.1	374.7	29.60	3.51	45.38	21.51
CH3	D13	410.25	410.48	52.44	4.32	11.79	31.45
CH3	D16	418.44	419.04	54.12	3.14	21.62	21.12
CH3	D18	421.46	422.06	53.88	2.05	26.58	17.49
CH4	D1	381.6	382.31	42.37	1.13	42.25	14.25
CH4	D3	438.25	438.6	11.57	2.27	81.96	4.21
CH4	D7	451.19	451.77	52.22	1.99	18.33	27.46
CH4	D15	479.97	480.52	53.20	2.50	17.16	27.13
CH4	D18	488.31	488.85	60.61	1.34	22.55	15.50
CH5	1	247.38	248.11	50.94	1.85	24.56	22.65
CH5	2	283.29	283.54	42.50	2.43	48.50	6.57
CH5	5	327.09	329.78	42.83	2.21	31.35	23.61
CH5	9	335.57	336.6	59.25	1.37	17.26	22.11
CH5	11	343.52	344.56	32.30	2.27	57.05	8.38
CH6	D2	319.78	320.37	28.41	5.99	42.21	23.38
CH6	D8	329.01	329.56	44.04	5.27	16.07	34.62
CH6	D13	340.22	340.8	49.41	4.98	13.60	32.00
CH6	D16	356.27	356.86	21.30	2.42	63.10	13.18
CH7	2G	404.28	404.88	31.01	6.36	29.78	32.85
CH7	11G	432.92	433.51	47.81	4.78	13.91	33.51
CH7	16G	440.22	440.82	44.95	3.52	22.65	28.88
CH7	21G	462.81	463.09	51.33	3.72	12.91	32.05
CH7	25G	485.62	486.22	67.18	1.30	22.10	9.42
CH8	D2	374.29	374.67	33.99	3.36	29.07	33.58
CH8	D5	386.81	387.41	46.15	3.15	22.79	27.91
CH8	D12	391.07	391.66	33.64	2.66	46.71	16.99
CH9	D2	406.4	407	34.21	3.81	39.94	22.04
CH9	D8	421.3	421.9	34.37	1.52	58.09	6.03
CH9	D18	444.6	445.2	41.97	1.91	40.61	15.51
CH9	D28	504.8	505.4	16.38	3.40	74.27	5.95
CH9	D31	521.2	521.8	53.46	2.07	26.64	17.82

APPENDIX E: Passey's method input parameters & calculated TOC results.

Well	Sample No.	Top Depth (m)	Bottom Depth (m)	Density (g/cc)	Gamma (API-GR)	Lateral (ohm-m)	Sonic (usec/m)	LOM	DLogR	TOCd (%)	SLogR	TOCs (%)	Fixed Carbon (%)	Comments
CH1	1_2G	246.12	246.59	1.45	57.63	77.98	401.83	7.72	3.52	34.65	2.93	28.83	43.49	CD: Pyrite, calcite
CH1	1_4G	268.8	269.4	1.43	66.53	146.50	410.58	7.86	3.83	35.73	3.38	31.49	42.82	CD: Pyrite, sideritic
CH1	1_5G	275.5	275.7	1.27	52.76	188.63	418.81	7.96	4.36	39.20	3.65	32.84	42.84	CD: Pyrite nodules
CH1	1_6G	277.76	278.35	1.36	63.74	191.38	423.49	7.86	4.13	38.48	3.75	34.98	39.46	CD: Pyritic
CH1	1_8G	279.9	280.11	1.94	161.49	77.26	358.12	8.00	2.28	20.12	2.05	18.11	49.62	CD-CM1: Pyrite, calcite
CH2	D3	257.99	258.6	1.55	42.21	61.61	397.38	7.82	3.42	32.49	2.74	25.98	34.82	CD: Pyrite, sideritic
CH2	D7	272.66	273.25	1.61	73.20	41.96	410.64	9.21	2.77	15.27	2.84	15.65	42.78	CD-C3: Pyrite, calcite
CH2	D9	276.19	276.42	1.33	79.06	23.76	433.49	12.20	3.20	5.53	3.05	5.26	60.81	C3
DOLERITE: 297.2-346.9 m														
CH2	D11	357.55	357.85	1.89	209.62	78.16	357.75	12.38	2.31	3.73	2.05	3.30	46.02	CR
CH3	D5	364.37	364.67	1.29	51.43	50.12	403.06	9.47	3.72	18.58	2.76	13.78	45.84	CD: Calcite, siderite
CH3	D12	374.1	374.7	1.33	40.74	74.74	411.89	8.10	3.80	32.35	3.11	26.52	29.60	CD: Pyrite, sideritic
CH3	D13	410.25	410.48	1.67	107.37	36.00	404.16	8.64	2.64	18.23	2.64	18.20	52.44	CD-C4: Calcite veins
CH3	D16	418.44	419.04	1.74	265.39	36.63	392.72	9.85	2.46	10.60	2.42	10.40	54.12	CM2: Pyrite
CH3	D18	421.46	422.06	1.50	155.00	45.55	422.10	11.72	3.17	6.59	3.10	6.45	53.88	CM2: Pyrite, calcite
DOLERITE: 431.7-460.7 m														
CH4	D1	381.6	382.31	1.87	88.60	21.69	340.27	13.54	2.09	2.15	1.46	1.50	42.37	Baked
DOLERITE: 392.3-426.5 m														
CH4	D3	438.25	438.6	1.83	83.73	0.44	401.64	19.26	0.48	0.05	0.99	0.11	11.57	Pyrite, sideritic
CH4	D7	451.19	451.77	1.27	49.54	39.29	387.59	9.52	3.83	18.79	2.67	13.08	52.22	CD-C3: Pyrite, calcite
CH4	D15	479.97	480.52	1.36	65.53	55.77	336.53	9.64	3.77	17.59	1.80	8.39	53.20	CM2-C4: Calcite
CH4	D18	488.31	488.85	1.68	134.33	79.87	383.96	12.45	3.11	4.87	2.90	4.55	60.61	C3-C4: Pyrite, calcite
DOLERITE: 505.5-507.9 m														
CH5	1	247.38	248.11	1.72	73.78	18.36	397.97	10.19	2.50	9.43	2.08	7.85	50.94	CD-CM2
DOLERITE: 268.4-281.8 m														
CH5	2	283.29	283.54	2.02	89.43	-0.31	357.92	19.25	#NUM!	#NUM!	#NUM!	#NUM!	42.50	Baked
DOLERITE: 294.3-295.1 m														
DOLERITE: 311.7-314.2 m														
CH5	5	327.09	329.78	1.58	83.23	68.18	416.62	11.76	3.42	7.00	3.02	6.19	42.83	C4-CM1: Calcite
CH5	9	335.57	336.6	1.46	86.25	79.88	423.43	11.07	3.77	10.10	3.22	8.64	59.25	C4-CM2
CH5	11	343.52	344.56	1.91	146.78	27.45	394.95	19.26	2.18	0.24	2.19	0.24	32.30	CM1
DOLERITE: 350.5-351.9 m														
DOLERITE: 353.6-381.8 m														
CH6	D2	319.78	320.37	1.55	73.73	82.88	391.12	7.86	3.45	44.97	2.90	37.77	28.41	C3
CH6	D8	329.01	329.56	1.56	88.07	82.53	384.60	8.05	3.42	44.58	2.76	36.05	44.04	C3: Sideritic
CH6	D13	340.22	340.8	1.31	22.16	141.40	420.54	8.46	4.29	55.93	3.72	48.47	49.41	C3: Sideritic
CH6	D16	356.27	356.86	1.80	217.33	27.65	344.46	8.68	2.34	30.58	1.49	19.38	21.30	CD
DOLERITE: 374.8-375.6 m														
CH7	2G	404.28	404.88	1.47	22.12	45.83	386.17	8.00	3.67	32.40	2.78	24.60	31.01	CD: Calcite, siderite
CH7	11G	432.92	433.51	1.29	34.21	74.16	410.42	8.19	4.32	35.57	3.48	28.61	47.81	C4: Pyrite, sideritic
CH7	16G	440.22	440.82	1.23	33.22	56.78	419.81	8.19	4.35	35.74	3.55	29.20	44.95	C4: Calcite, siderite
CH7	21G	462.81	463.09	1.68	105.04	40.01	396.05	8.23	3.08	24.91	2.92	23.62	51.33	C4: Sideritic
CH7	25G	485.62	486.22	1.40	49.23	58.27	411.72	18.13	3.94	0.68	3.40	0.59	67.18	CD-C4: Calcite veins
DOLERITE: 500.4-522.7 m														
CH8	D2	374.29	374.67	1.46	32.41	31.14	394.38	7.54	3.14	33.20	2.54	26.85	33.99	CD: Pyrite
CH8	D5	386.81	387.41	1.62	78.48	31.34	410.62	8.55	2.74	19.54	2.86	20.45	46.15	CD: Pyrite, calcite
CH8	D12	391.07	391.66	1.50	68.02	52.54	407.06	9.77	3.25	14.45	3.02	13.40	33.64	CD: Calcite cleats
DOLERITE: 419-491.4														
CH9	D2	406.4	407	1.68	56.33	19.73	398.63	8.05	2.27	19.70	2.79	24.19	34.21	CD: Calcite cleats
DOLERITE: 419.6-420.9 m														
CH9	D8	421.3	421.9	2.17	94.97	24.80	302.51	17.81	1.13	0.22	0.97	0.19	34.37	CR: Pyrite
CH9	D18	444.6	445.2	1.57	134.03	71.33	350.62	11.38	3.10	7.37	2.39	5.67	41.97	CM2-CR: Pyrite
DOLERITE: 455.9-498.4 m														
CH9	D28	504.8	505.4	1.97	173.00	1.40	418.45	19.00	0.40	0.05	2.04	0.25	16.38	CM2-CR: Pyrite
CH9	D31	521.2	521.8	1.44	58.14	66.32	363.02	13.44	3.38	3.61	2.60	2.77	53.46	CD: Pyrite nodules
DOLERITE: 525.9-542.7														

Lithology abbreviations in Appendix E:

CB= Coal bright (>90% bright), C1= Coal bright with dull bands (60-90% bright), C2= Coal interbanded dull and bright (40-60% bright), C3= Coal dull with frequent bright bands (10-40% bright), C4 =coal dull with minor bright bands (1-10% bright), CD= Coal dull (<1% bright), CR= Stony coal, CM1= Carbonaceous mudstone and CM2= Coaly mudstone.

List of used abbreviations

Abbreviation	Name
CBM	Coalbed Methane
%Ro	Vitrinite Reflectance
%TOC	Total Organic carbon
LOM	Level of Organic Metamorphism
HA	Heat Affected
Non-HA	Non-Heat Affected
SlogR,DlogR	Passey's number from sonic, density (fractional)
RESD	Deep resistivity in any zone (ohm-m)
RESDbase,DTCbase, DENSbase	Deep resistivity, sonic or density baseline in non-source rock (ohm-m)
DTC	Compressional; sonic log reading in any zone (usec/ft)
DENS	Density in non-source rock (gm/cc).
TOCs,d	Total organic carbon from Passey's method using sonic or density logs (weight fraction)
IP	Interactive Petrophysics™ (Software)